

1 Scattering of light by an array of atoms

In our experiment we observe the scattering of photons from atoms confined in an optical lattice, here we treat this situation by first obtaining the field scattered from a single atom and then summing the field contributions from all the atoms coherently at the location of our detector. The main goal of this document is to find the connection between the intensity that we measure at our cameras and the spin structure factor as calculated by the theorists in our collaboration.

1.1 Electric field and intensity due to a single atom

To calculate the scattered field, one uses the source-field expression, which relates the radiated field to the dipole moment of the emitting two-level system, this is derived in the standard textbooks [1, 2]. The field at the position of the detector \mathbf{r}_D is given by

$$E^{(+)}(\mathbf{r}_D, t) = \eta e^{-i\omega_L(t-r_D/c)} \sigma_- \left(t - \frac{r_D}{c} \right) \quad (1)$$

where η is a proportionality factor that we will address later on. The time-averaged intensity at the detector is

$$\begin{aligned} \langle I(t) \rangle &= \langle E^{(-)}(\mathbf{r}_D, t) E^{(+)}(\mathbf{r}_D, t) \rangle \\ &= |\eta|^2 \langle \sigma_+(t - r_D/c) \sigma_-(t - r_D/c) \rangle \end{aligned} \quad (2)$$

In the steady state $\langle \sigma_+(t) \sigma_-(t) \rangle$ does not depend on t , so

$$\begin{aligned} \langle I(t) \rangle &= |\eta|^2 \langle \sigma_+ \sigma_- \rangle \\ &= |\eta|^2 \rho_{ee} \end{aligned} \quad (3)$$

We can write the σ_{\pm} operators of the atoms as

$$\sigma_{\pm} = \langle \sigma_{\pm} \rangle + \delta\sigma_{\pm} \quad (4)$$

which defines $\delta\sigma$. Writing σ_{\pm} in this way allows us to distinguish between two components in the radiated light: the radiation of the average dipole $\langle \sigma_{\pm} \rangle$ which is the radiation of a classical oscillating dipole with a phase that is well defined relative to the incident laser field, and the radiation from the $\delta\sigma_{\pm}$ component which does not have a phase that is well defined relative to the incident field because it comes from the fluctuating part of the atomic dipole. The intensity is then a sum of coherent and incoherent parts

$$I = \eta^2 \langle \sigma_+ \rangle \langle \sigma_- \rangle + \eta^2 \langle \delta\sigma_+ \delta\sigma_- \rangle \quad (5)$$

where we have used the fact that by definition $\langle \delta\sigma_{\pm} \rangle = 0$. The first and second terms of this equation are the coherent and incoherent intensity and can be calculated by using the steady-state solutions to the optical Bloch equations:

$$\langle \sigma_{\pm} \rangle = u \pm iv \quad (6)$$

$$u = \frac{\Delta}{\Gamma\sqrt{s_0/2}} \frac{s}{1+s} \quad (7)$$

$$v = \frac{1}{2\sqrt{s_0/2}} \frac{s}{1+s} \quad (8)$$

$$(9)$$

where s is the saturation parameter for an incident probe with intensity I_p and detuning Δ :

$$s = \frac{2I_p/I_{\text{sat}}}{1 + 4(\Delta/\Gamma)^2} \equiv \frac{s_0}{1 + 4(\Delta/\Gamma)^2} \quad (10)$$

and $I_{\text{sat}} = \frac{\hbar k^3 c \Gamma}{6\pi}$ for a transition with linewidth Γ .

The coherent and incoherent parts of the intensity are

$$\begin{aligned} \frac{1}{\eta^2} I_{\text{coh}} &= \frac{1}{2} \frac{s}{(1+s)^2} = \rho_{ee} \frac{1}{1+s} \\ \frac{1}{\eta^2} I_{\text{incoh}} &= \langle \sigma_+ \sigma_- \rangle - \langle \sigma_+ \rangle \langle \sigma_- \rangle = \frac{1}{2} \frac{s^2}{(1+s)^2} = \rho_{ee} \frac{s}{1+s} \end{aligned} \quad (11)$$

Note that if we add them up we get the familiar result $I = \eta^2 \rho_{ee}$, where the total intensity is simply proportional to the population of the excited state.

1.2 Scattering cross-section

Now we will turn onto the evaluation of η , the proportionality factor between the field at \mathbf{r}_D and the emitting dipole. We start by considering the transition matrix element between the following initial and final states of the atom+photon system:

$$\begin{aligned} |\varphi_i\rangle &= |g; \mathbf{k}\varepsilon\rangle \\ |\varphi_f\rangle &= |g'; \mathbf{k}'\varepsilon'\rangle \end{aligned} \quad (12)$$

These states represent the absorption and re-emission of a single photon by the atom, with two possibly different initial and final photon states, and two possibly different initial and final atom ground states.

The transition rate to from $i \rightarrow f$ is given by [2]

$$w_{fi} = \frac{2\pi}{\hbar} |\mathcal{T}_{fi}|^2 \delta(E_f - E_i) \quad (13)$$

where

$$\mathcal{T}_{fi} = \frac{\langle g'; \mathbf{k}'\varepsilon' | H'_I | e; 0 \rangle \langle e; 0 | H'_I | g; \mathbf{k}\varepsilon \rangle}{\hbar\omega - \hbar\omega_0 + i\hbar(\Gamma/2)} \quad (14)$$

and the interaction Hamiltonian is

$$H'_I = -\mathbf{d} \cdot \mathbf{E}_\perp(\mathbf{r}) \quad (15)$$

with

$$\mathbf{E}_\perp(\mathbf{r}) = i \sum_j \left[\frac{\hbar\omega_j}{2\varepsilon_0 L^3} \right]^{1/2} \left(\hat{a}_j \varepsilon_j e^{i\mathbf{k}_j \cdot \mathbf{r}} - \hat{a}_j^* \varepsilon_j^* e^{-i\mathbf{k}_j \cdot \mathbf{r}} \right) \quad (16)$$

Note: In the equations above we use the notation in [2], see Exercise 5 on pg. 530. SI units are used there, as revealed by the presence of ϵ_0 in the expression for $\mathbf{E}_\perp(\mathbf{r})$. The intermediate state in the photon absorption-emission cycle is denoted as $|e; 0\rangle$.

Using the expressions for H'_I and $\mathbf{E}_\perp(\mathbf{r})$ we obtain for the matrix element

$$\langle e; 0 | H'_I | g; \mathbf{k}\varepsilon \rangle = -i \sqrt{\frac{\hbar\omega}{2\varepsilon_0 L^3}} \langle e | (\mathbf{d} \cdot \varepsilon^*) e^{-i\mathbf{k} \cdot \mathbf{r}} | g \rangle \quad (17)$$

At this point the textbook treatment usually assumes that the atom is at the origin and that the size

of the atom wavefunction is very small compared to $|\mathbf{k}|^{-1}$, and so the exponential inside the matrix element typically does not show up. In our case the atom is in a lattice site and its center of mass state is one of the harmonic oscillator states of a lattice well, which is large enough that the exponential term cannot be neglected.

The states $|e\rangle$ and $|g\rangle$ include the center of mass and internal states of the atom. We separate the center of mass part, but keep the labels e, g for the internal states. We denote the center of mass initial and final states as $|u\rangle$ and $|u'\rangle$ respectively, and the center of mass state of the intermediate excited state as $|v\rangle$. Also, we assume that the final internal state of the atom is the same as the initial state, $g' = g$. These matrix element becomes

$$\langle e; 0 | H'_I | g; \mathbf{k}\epsilon \rangle = -i\sqrt{\frac{\hbar\omega}{2\varepsilon_0 L^3}} \underbrace{\langle e | \mathbf{d} \cdot \boldsymbol{\epsilon}^* | g \rangle}_{\text{internal}} \underbrace{\langle v | e^{-i\mathbf{k} \cdot \mathbf{r}} | u \rangle}_{\text{external}} \quad (18)$$

and similarly

$$\langle g; \mathbf{k}'\epsilon' | H'_I | e; 0 \rangle = i\sqrt{\frac{\hbar\omega'}{2\varepsilon_0 L^3}} \langle g | \mathbf{d} \cdot \boldsymbol{\epsilon}' | e \rangle \langle u' | e^{i\mathbf{k}' \cdot \mathbf{r}} | v \rangle \quad (19)$$

Collecting the above and summing over all possible intermediate center of mass states we have

$$\mathcal{T}_{fi} = \sum_v \frac{\sqrt{\omega\omega'}}{2\varepsilon_0 L^3} \frac{\langle g | \mathbf{d} \cdot \boldsymbol{\epsilon}' | e \rangle \langle e | \mathbf{d} \cdot \boldsymbol{\epsilon}^* | g \rangle \langle u' | e^{i\mathbf{k}' \cdot \mathbf{r}} | v \rangle \langle v | e^{-i\mathbf{k} \cdot \mathbf{r}} | u \rangle}{\omega - \omega_0 + i(\Gamma/2)} \quad (20)$$

Note that the sum can be taken out using the closure relation $\sum_v |v\rangle\langle v| = \mathbb{1}$.

In our experiment we are driving a sigma-minus transition so

$$\begin{aligned} \langle e | \mathbf{d} \cdot \boldsymbol{\epsilon}^* | g \rangle &= d_- (\boldsymbol{\epsilon}_- \cdot \boldsymbol{\epsilon}^*) \\ \langle g | \mathbf{d} \cdot \boldsymbol{\epsilon}' | e \rangle &= d_-^* (\boldsymbol{\epsilon}_+ \cdot \boldsymbol{\epsilon}') \end{aligned} \quad (21)$$

where the dipole matrix element, d_- , is related to the linewidth as

$$|d_-|^2 = 3\pi\varepsilon_0\hbar \left(\frac{c}{\omega_0}\right)^3 \Gamma \quad (22)$$

Plugging this in, using $\omega' \approx \omega \approx \omega_0$ in the numerator of Eq. 20 and $\omega - \omega_0 = \Delta$ in the denominator leads to

$$\mathcal{T}_{fi} = \frac{3}{k^2} \frac{\pi\hbar c}{L^3} (\boldsymbol{\epsilon}_+ \cdot \boldsymbol{\epsilon}') (\boldsymbol{\epsilon}^* \cdot \boldsymbol{\epsilon}_-) \frac{\Gamma/2}{\Delta + i(\Gamma/2)} \langle u' | e^{i(\mathbf{k}' - \mathbf{k}) \cdot \mathbf{r}} | u \rangle \quad (23)$$

The scattering rate of photons towards a certain solid angle Ω' is obtained by summing the transition rate, w_{fi} , over all possible final states. This is done by using the density of states

$$\rho(\hbar ck') \hbar c dk' d\Omega' = \frac{L^3}{8\pi^3} k'^2 dk' d\Omega' \quad (24)$$

to replace a sum over k' with an integral:

$$\begin{aligned} \sum_f w_{fi} &= \frac{2\pi}{\hbar} d\Omega' \int_0^\infty \frac{k'^2 dk'}{(2\pi/L^3)^3} |\mathcal{T}_{fi}|^2 \delta(\hbar ck' - \hbar ck) \\ &= d\Omega' \frac{9}{4k^2} \frac{c}{L^3} |(\boldsymbol{\epsilon}_+ \cdot \boldsymbol{\epsilon}') (\boldsymbol{\epsilon}^* \cdot \boldsymbol{\epsilon}_-)|^2 \frac{(\Gamma/2)^2}{\Delta^2 + (\Gamma/2)^2} \left| \langle u' | e^{i(\mathbf{k}' - \mathbf{k}) \cdot \mathbf{r}} | u \rangle \right|^2 \end{aligned} \quad (25)$$

We consider the flux corresponding to the state of the initial photon, $\phi = c/L^3$, and define the differential cross section which allows us to get rid of the quantization volume L^3 :

$$\frac{d\sigma}{d\Omega' \phi} = \frac{\sum_f w_{fi}}{d\Omega' \phi} = \frac{9}{4k^2} |(\boldsymbol{\varepsilon}_+ \cdot \boldsymbol{\varepsilon}')(\boldsymbol{\varepsilon}^* \cdot \boldsymbol{\varepsilon}_-)|^2 \frac{(\Gamma/2)^2}{\Delta^2 + (\Gamma/2)^2} \left| \langle u' | e^{i(\mathbf{k}' - \mathbf{k}) \cdot \mathbf{r}} | u \rangle \right|^2 \quad (26)$$

From here we can write down the intensity on a detector located at \mathbf{r}_D in the direction of $d\Omega'$ as ¹

$$\begin{aligned} I &= \frac{1}{r_D^2} \frac{d\sigma}{d\Omega'} I_p = \frac{1}{r_D^2} \frac{d\sigma}{d\Omega'} s_0 (I_{\text{sat}}/2) = \frac{1}{r_D^2} \frac{d\sigma}{d\Omega'} s_0 \frac{\hbar k^3 c \Gamma}{12\pi} \\ &= \underbrace{\frac{\hbar c k \Gamma}{r_D^2} \frac{9}{24\pi} |(\boldsymbol{\varepsilon}_+ \cdot \boldsymbol{\varepsilon}')(\boldsymbol{\varepsilon}^* \cdot \boldsymbol{\varepsilon}_-)|^2 \left| \langle u' | e^{i(\mathbf{k}' - \mathbf{k}) \cdot \mathbf{r}} | u \rangle \right|^2}_{|\eta^2|} \underbrace{\frac{s_0/2}{4(\Delta/\Gamma)^2 + 1}}_{\rho_{ee}} \end{aligned} \quad (27)$$

In this last product we identify η and ρ_{ee} (in the limit of low intensity). Comparing with Eq. 11 we can write down an expression for η ,

$$\eta = \left[\frac{\hbar c k \Gamma}{r_D^2} \frac{9}{24\pi} \right]^{1/2} (\boldsymbol{\varepsilon}_+ \cdot \boldsymbol{\varepsilon}')(\boldsymbol{\varepsilon}^* \cdot \boldsymbol{\varepsilon}_-) \langle u' | e^{i(\mathbf{k}' - \mathbf{k}) \cdot \mathbf{r}} | u \rangle \quad (28)$$

With an exact expression for η we can obtain the field radiated by each atom and proceed to sum the field coherently for a collection of atoms.

1.3 Summation for a collection of atoms

For a collection of atoms, the resulting field is the sum of the field produced by each individual atom, so we have for the intensity

$$\begin{aligned} I(t) &= \left\langle \left(\sum_m E_m^{(-)}(\mathbf{r}_D, t) \right) \left(\sum_n E_n^{(+)}(\mathbf{r}_D, t) \right) \right\rangle \\ &= \left\langle \sum_{mn} \eta_m^* \eta_n e^{i\omega_L(r_n - r_m)/c} \sigma_{m+}(t - r_m/c) \sigma_{n-}(t - r_n/c) \right\rangle \end{aligned} \quad (29)$$

The atomic dipole operators can be shifted in time as

$$\begin{aligned} \sigma_{m+}(t - r_m/c) \sigma_{n-}(t - r_n/c) &= \sigma_{m+}(t' + r_n/c - r_m/c) \sigma_{n-}(t') \\ &= e^{-i\omega_L(r_n - r_m)/c} \sigma_{m+}(t') \sigma_{n-}(t') \end{aligned} \quad (30)$$

to obtain

$$I = \sum_{mn} \eta_m^* \eta_n \langle \sigma_{m+}(t') \sigma_{n-}(t') \rangle \quad (31)$$

¹Later on we will sum over output polarizations and final center of mass states of the atom, since our detection is insensitive to them.

Dropping the time dependence and using $\sigma = \langle \sigma \rangle + \delta\sigma$, as we did above to obtain the coherent and incoherent parts of the intensity, we obtain

$$\begin{aligned} I &= \sum_{mn} \eta_m^* \eta_n (\langle \sigma_{m+} \rangle \langle \sigma_{n-} \rangle + \langle \delta\sigma_{m+} \delta\sigma_{n-} \rangle) \\ &= \sum_{mn} \eta_m^* \eta_n \langle \sigma_{m+} \rangle \langle \sigma_{n-} \rangle + \sum_n |\eta_n|^2 \langle \delta\sigma_{n+} \delta\sigma_{n-} \rangle \end{aligned} \quad (32)$$

The last term here is the incoherently scattered part due to the fluctuating fraction δS_\pm of the atomic dipole. The cross terms do not appear in this sum because $\langle \delta\sigma_{m+} \delta\sigma_{n-} \rangle = 0$ for $m \neq n$; this part is identified as the incoherent scattering.

The steady state solutions of the optical Bloch equations are used again to evaluate the expectation values:

$$\begin{aligned} I &= \sum_{mn} \eta_m^* \eta_n \left(\frac{\Delta_m}{\Gamma \sqrt{s_0/2}} \frac{s_m}{1+s_m} + i \frac{1}{2\sqrt{s_0/2}} \frac{s_m}{1+s_m} \right) \left(\frac{\Delta_n}{\Gamma \sqrt{s_0/2}} \frac{s_n}{1+s_n} - i \frac{1}{2\sqrt{s_0/2}} \frac{s_n}{1+s_n} \right) \\ &\quad + \sum_n |\eta_n|^2 \frac{1}{2} \frac{s_n^2}{(1+s_n)^2} \end{aligned} \quad (33)$$

From this point on we will specify the detuning in units of the linewidth, so we make the replacement $\Delta/\Gamma \rightarrow \Delta$.

$$I = \sum_{mn} \eta_m^* \eta_n \frac{s_m s_n}{s_0(1+s_m)(1+s_n)} \left(2\Delta_m \Delta_n + i\Delta_n - i\Delta_m + \frac{1}{2} \right) + \sum_n |\eta_n|^2 \frac{1}{2} \frac{s_n^2}{(1+s_n)^2} \quad (34)$$

We split up the first sum into $m \neq n$ and $m = n$ parts to obtain

$$\begin{aligned} I &= \sum_{m \neq n} \eta_m^* \eta_n \frac{s_m s_n}{s_0(1+s_m)(1+s_n)} \left(2\Delta_m \Delta_n + i\Delta_n - i\Delta_m + \frac{1}{2} \right) \\ &\quad + \sum_n |\eta_n|^2 \frac{s_n^2}{s_0(1+s_n)^2} \left(2\Delta_n^2 + \frac{1}{2} \right) + \sum_n |\eta_n|^2 \frac{1}{2} \frac{s_n^2}{(1+s_n)^2} \\ &= \sum_{m \neq n} \eta_m^* \eta_n \frac{s_m s_n}{s_0(1+s_m)(1+s_n)} \left(2\Delta_m \Delta_n + i\Delta_n - i\Delta_m + \frac{1}{2} \right) + \frac{1}{2} \sum_n |\eta_n|^2 \frac{s_n}{1+s_n} \end{aligned} \quad (35)$$

We now focus our attention on the terms $\eta_m^* \eta_n$ ($m \neq n$) and $|\eta_n|^2$. We start with the latter

$$|\eta_n|^2 = \frac{\hbar c k \Gamma}{r_D^2} \frac{9}{24\pi} |(\boldsymbol{\varepsilon}_+ \cdot \boldsymbol{\varepsilon}')(\boldsymbol{\varepsilon}^* \cdot \boldsymbol{\varepsilon}_-)|^2 \langle u | e^{-i(\mathbf{k}'-\mathbf{k}) \cdot \mathbf{r}_n} | u' \rangle \langle u' | e^{i(\mathbf{k}'-\mathbf{k}) \cdot \mathbf{r}_n} | u \rangle \quad (36)$$

and notice that we have to sum over output polarizations $\boldsymbol{\varepsilon}'$ and final center of mass states u' , since our detector does not care about either. We obtain

$$\begin{aligned} \sum_{\boldsymbol{\varepsilon}' u'} |\eta_n|^2 &= \sum_{u'} \frac{\hbar c k \Gamma}{r_D^2} \frac{9}{24\pi} \sum_{\boldsymbol{\varepsilon}'} |(\boldsymbol{\varepsilon}_+ \cdot \boldsymbol{\varepsilon}')(\boldsymbol{\varepsilon}^* \cdot \boldsymbol{\varepsilon}_-)|^2 \langle u | e^{-i(\mathbf{k}'-\mathbf{k}) \cdot \mathbf{r}_n} | u' \rangle \langle u' | e^{i(\mathbf{k}'-\mathbf{k}) \cdot \mathbf{r}_n} | u \rangle \\ &= \frac{\hbar c k \Gamma}{r_D^2} \frac{9}{24\pi} \Lambda \langle u | e^{-i(\mathbf{k}'-\mathbf{k}) \cdot \mathbf{r}_n} e^{i(\mathbf{k}'-\mathbf{k}) \cdot \mathbf{r}_n} | u \rangle \\ &= \frac{\hbar c k \Gamma}{r_D^2} \frac{9}{24\pi} \Lambda \end{aligned} \quad (37)$$

where we have used the closure relation $\sum_{u'} |u'\rangle\langle u'| = \mathbb{1}$, and have defined for brevity

$$\Lambda = \sum_{\epsilon'} |(\epsilon_+ \cdot \epsilon')(\epsilon \cdot \epsilon_-)|^2 \quad (38)$$

Similarly, for $\eta_m^* \eta_n$

$$\sum_{\epsilon' u'_m u'_n} \eta_m^* \eta_n = \frac{\hbar c k \Gamma}{r_D^2} \frac{9}{24\pi} \Lambda \sum_{u'_m u'_n} \langle u_m | e^{-i(\mathbf{k}' - \mathbf{k}) \cdot \mathbf{r}_m} | u'_m \rangle \langle u'_n | e^{i(\mathbf{k}' - \mathbf{k}) \cdot \mathbf{r}_n} | u_n \rangle \quad (39)$$

In this case we cannot use the closure relation because n, m refer to different atoms. We simplify the treatment by considering only final center of mass states that are the same as the initial state: $u' = u$. In a deep lattice the number of scattering events in which the atom does not return to its original center of mass state are suppressed by a factor equal to the square of the Lamb-Dicke parameter:

$$\eta_{LD}^2 = \frac{E_R}{\hbar \omega_{\text{lattice}}} = \frac{1}{2\sqrt{V_0/E_R}} \quad (40)$$

In our experiment we use a lattice depth $V_0 = 20E_R$ for the scattering measurement, so we have $\eta_{LD}^2 = 0.11$. This means that one in every about 9 scatters will take the atom to a different center of mass state. As long as we keep the number of photons scattered small enough we can consider only $u'_m = u_m$ and $u'_n = u_n$ in Eq. 39. The center of mass state of the atoms is the ground state of the single lattice site harmonic oscillator, which we denote as $|0\rangle$. This leaves us with

$$\sum_{\epsilon'} \eta_m^* \eta_n = \frac{\hbar c k \Gamma}{r_D^2} \frac{9}{24\pi} \Lambda \langle 0_m | e^{-i(\mathbf{k}' - \mathbf{k}) \cdot \mathbf{r}_m} | 0_m \rangle \langle 0_n | e^{i(\mathbf{k}' - \mathbf{k}) \cdot \mathbf{r}_n} | 0_n \rangle \quad (41)$$

1.3.1 Debye-Waller factor

For each center of mass expectation value we perform a translation \mathbf{R}_m of the coordinate system such that the position of the m^{th} atom has a zero expectation value $\langle \mathbf{r}_m \rangle = 0$. A phase factor comes out that depends on the position \mathbf{R}_m of the lattice site in which the atom is located:

$$\langle 0_m | e^{-i(\mathbf{k}' - \mathbf{k}) \cdot \mathbf{r}_m} | 0_m \rangle = e^{-i(\mathbf{k}' - \mathbf{k}) \cdot \mathbf{R}_m} \langle 0_m | e^{-i(\mathbf{k}' - \mathbf{k}) \cdot \mathbf{r}_m} | 0_m \rangle \quad (42)$$

We then use the equality $\langle e^{\hat{A}} \rangle = e^{\frac{1}{2}\langle \hat{A}^2 \rangle}$, which is valid for a simple harmonic oscillator, where \hat{A} is any linear combination of displacement and momentum operators of the oscillator. This leaves us with

$$\begin{aligned} \langle 0_m | e^{-i(\mathbf{k}' - \mathbf{k}) \cdot \mathbf{r}_m} | 0_m \rangle &= e^{-i(\mathbf{k}' - \mathbf{k}) \cdot \mathbf{R}_m} e^{-\frac{1}{2}\langle [(\mathbf{k}' - \mathbf{k}) \cdot \mathbf{r}_m]^2 \rangle} \\ &= e^{-i\mathbf{Q} \cdot \mathbf{R}_m} e^{-\frac{1}{2}\langle [\mathbf{Q} \cdot \mathbf{r}_m]^2 \rangle} \\ &= e^{-i\mathbf{Q} \cdot \mathbf{R}_m} \prod_{i=x,y,z} e^{-\frac{1}{2}Q_i^2 \langle r_{mi}^2 \rangle} \\ &= e^{-i\mathbf{Q} \cdot \mathbf{R}_m} e^{-W} \end{aligned} \quad (43)$$

where we have defined the momentum transfer $\mathbf{Q} = \mathbf{k}' - \mathbf{k}$, and the Debye-Waller factor e^{-2W} .

Putting this back in the expression for $\eta_m^* \eta_n$ we get

$$\sum_{\epsilon'} \eta_m^* \eta_n = \frac{\hbar c k \Gamma}{r_D^2} \frac{9}{24\pi} \Lambda e^{i\mathbf{Q} \cdot (\mathbf{R}_n - \mathbf{R}_m)} e^{-2W} \quad (44)$$

And if we now return to the expression for the intensity at the detector we have

$$I = \frac{\hbar ck\Gamma}{r_D^2} \frac{9\Lambda}{24\pi} \left[\sum_{m \neq n} \frac{e^{i\mathbf{Q}(\mathbf{R}_n - \mathbf{R}_m)} e^{-2W} s_m s_n}{s_0(1+s_m)(1+s_n)} \left(2\Delta_m \Delta_n + i\Delta_n - i\Delta_m + \frac{1}{2} \right) + \frac{1}{2} \sum_n \frac{s_n}{1+s_n} \right] \quad (45)$$

For large time-of-flight, where the Debye-Waller factor goes to zero due to large extent of the expanding atom wavefunctions, this formula reduces to the standard uncorrelated scattering for N atoms, $I \propto N\rho_{ee}$ with $\rho_{ee} = \frac{1}{2}\frac{s}{1+s}$. We can evaluate the total photon scattering rate $\Gamma_{\text{scatt}} = \frac{1}{\hbar ck} \int I r_D^2 d\Omega$, for which we use $\int \Lambda d\Omega = \frac{8\pi}{3}$ and obtain

$$\Gamma_{\text{scatt}} = \Gamma \frac{N}{2} \frac{s}{1+s} = N\Gamma\rho_{ee} \quad (46)$$

This result gives a consistency check on the prefactors that appear in Eq. 45.

1.4 Large detuning limit

We now look at the detuning dependent term in the $m \neq n$ part of the scattered intensity

$$\frac{s_m s_n}{(1+s_m)(1+s_n)} \left(2\Delta_m \Delta_n + i\Delta_n - i\Delta_m + \frac{1}{2} \right) \quad (47)$$

For a detuning such that $4\Delta_m^2, 4\Delta_n^2 \gg 1$ we have

$$\frac{s}{1+s} \approx \frac{s_0}{4\Delta^2 + s_0} \quad (48)$$

Furthermore, if we detune the light in between the two spin states then we can use, $\Delta_m^2 = \Delta^2$ and $\Delta_m = 2\Delta S_{zm}$, where $S_{zm} = \pm\frac{1}{2}$ is the spin state of the atom in site m . The four terms in the coherent part of the intensity go to

$$s_0^2 \frac{8\Delta^2 S_{zm} S_{zm}}{(4\Delta^2 + s_0)^2} \quad (49)$$

$$s_0^2 \frac{+2i\Delta S_{zn}}{(4\Delta^2 + s_0)^2} \quad (50)$$

$$s_0^2 \frac{-2i\Delta S_{zm}}{(4\Delta^2 + s_0)^2} \quad (51)$$

$$s_0^2 \frac{1/2}{(4\Delta^2 + s_0)^2} \quad (52)$$

The intensity at the detector becomes

$$I = \frac{\hbar ck\Gamma}{r_D^2} \frac{9}{24\pi} \Lambda \left[\frac{s_0 \Delta^2 e^{-2W}}{(4\Delta^2 + s_0)^2} \sum_{m \neq n} e^{i\mathbf{Q}(\mathbf{R}_n - \mathbf{R}_m)} \left(8S_{zm} S_{zn} + 2i\frac{S_{zn}}{\Delta} - 2i\frac{S_{zm}}{\Delta} + \frac{1}{2\Delta^2} \right) + \frac{1}{2} \sum_n \frac{s_0}{4\Delta^2 + s_0} \right] \quad (53)$$

There are two terms in the $m \neq n$ part that can be split up as

$$\frac{1}{\Delta} \sum_m e^{-i\mathbf{Q}\mathbf{R}_m} \sum_m e^{i\mathbf{Q}\mathbf{R}_n} S_{zn} \quad \frac{1}{\Delta} \sum_m e^{-i\mathbf{Q}\mathbf{R}_m} S_{zm} \sum_m e^{i\mathbf{Q}\mathbf{R}_n} \quad (54)$$

Since \mathbf{Q} cannot be a reciprocal lattice vector of the pure lattice and the spin lattice at the same time these products will at most be of order N/Δ and can be neglected. The resulting intensity at the detector is

$$I = \frac{\hbar c k \Gamma}{r_D^2} \frac{9\Lambda}{48\pi} \frac{\frac{s_0}{4\Delta^2}}{1 + \frac{s_0}{4\Delta^2}} \left[\frac{e^{-2W}}{1 + \frac{s_0}{4\Delta^2}} \left(\underbrace{4 \sum_{m \neq n} e^{i\mathbf{Q}(\mathbf{R}_n - \mathbf{R}_m)} S_{zm} S_{zn}}_{N(S_Q - 1)} + \underbrace{\frac{1}{4\Delta^2} \sum_{m \neq n} e^{i\mathbf{Q}(\mathbf{R}_n - \mathbf{R}_m)}}_{N(C_Q - 1)} \right) \right] \quad (55)$$

where we have identified the spin structure factor S_Q and the crystal structure factor C_Q which are defined as

$$S_Q = \frac{4}{N} \sum_{mn} e^{i\mathbf{Q}(\mathbf{R}_m - \mathbf{R}_n)} S_{zm} S_{zn} \quad (56)$$

$$C_Q = \sum_{mn} e^{i\mathbf{Q}(\mathbf{R}_m - \mathbf{R}_n)} \quad (57)$$

If $4\Delta^2 \gg 1$, the crystal structure factor term can be neglected when \mathbf{Q} is not a reciprocal lattice vector.

We consider a measurement of the intensity after a large time-of-flight (TOF), denoted as $I_{Q\infty}$. After TOF, the Debye-Waller factor goes to zero due to the expanding size of the atomic wavefunction, so we have

$$I_{Q\infty} = \frac{\hbar c k \Gamma}{r_D^2} \frac{9\Lambda}{48\pi} \frac{\frac{s_0}{4\Delta^2}}{1 + \frac{s_0}{4\Delta^2}} N \quad (58)$$

and therefore

$$\frac{I_Q}{I_{Q\infty}} = \frac{e^{-2W}}{1 + \frac{s_0}{4\Delta^2}} \left((S_Q - 1) + \frac{1}{4\Delta^2} (C_Q - 1) \right) + 1 \quad (59)$$

2 Measurement of the spin structure factor

The theorists in our collaboration calculate the spin structure factor, S , for a given value of the momentum transfer \mathbf{Q} . In Eq. 59 we neglect the crystal structure factor, since we do not detect at values of \mathbf{Q} that are near a reciprocal lattice vector of the simple cubic lattice.

We introduce the notation

$$\frac{I_Q}{I_{Q\infty}} \equiv i_Q \quad c \equiv \frac{e^{-2W}}{1 + \frac{s_0}{4\Delta^2}} \quad (60)$$

to obtain

$$i_Q = c(S_Q - 1) + 1 \quad (61)$$

For a measurement in a deep enough lattice ($e^{-2W} \rightarrow 1$) and with a low intensity probe ($s_0 \ll 4\Delta^2$)

the TOF normalized intensity and the structure factor are equivalent:

$$i_{\mathbf{Q}} = S_{\mathbf{Q}} \quad (62)$$

In our experiment we are using $s_0 \approx 15$ and $\Delta = 6.5$. We perform the measurement at a lattice depth of $20E_R$. For these parameters, and at the momentum transfer \mathbf{Q} sensitive to antiferromagnetic ordering we have

$$\begin{aligned} e^{-2W} &= 0.72 \\ 1 + \frac{s_0}{4\Delta^2} &= 1.18 \end{aligned} \quad (63)$$

$$S_{\mathbf{Q}} - 1 = 1.64 \times (i_{\mathbf{Q}} - 1) \quad (64)$$

2.1 Time-of-flight

If the atoms are released from the lattice before probing with the Bragg beam then we must consider the change in the Debye-Waller factor as the atomic wavefunctions expand. We recall that the Debye-Waller factor is defined as

$$e^{-2W} = \prod_{i=x,y,z} e^{-Q_i^2 \langle r_i^2 \rangle} \quad (65)$$

where Q_i is the i^{th} component of the momentum transfer $\mathbf{Q} = \mathbf{k}' - \mathbf{k}$, with \mathbf{k}' and \mathbf{k} the wave vectors of the outgoing and incoming light respectively. The time-of-flight dependence of the Debye-Waller factor is through the expanding size of the atomic wavefunctions. For an in-situ picture $\langle r_i^2 \rangle$ corresponds to the position variance of the harmonic oscillator ground state in a lattice site. After the atoms are released from the lattice the position variance satisfies

$$\begin{aligned} \langle r_i^2 \rangle_t &= \langle r_i^2 \rangle_0 + \frac{t^2}{m^2} \langle p_i^2 \rangle_0 \\ &= \langle r_i^2 \rangle_0 + \frac{t^2}{m^2} \frac{\hbar^2}{4 \langle r_i^2 \rangle_0} \end{aligned} \quad (66)$$

In a harmonic oscillator potential

$$\langle r^2 \rangle = \frac{\hbar}{2m\omega} \quad (67)$$

and for a lattice of depth $V_0 E_R$,

$$\langle r^2 \rangle = \frac{a^2}{2\pi^2 \sqrt{V_0}} \quad (68)$$

where a is the lattice spacing.

We then have for the Debye-Waller factor as a function of time-of-flight

$$\begin{aligned}
[e^{-2W}]_t &= \prod_{i=x,y,z} \exp \left[-Q_i^2 \left(\frac{a^2}{2\pi^2 \sqrt{V_0}} + \frac{h^2 \sqrt{V_0}}{8a^2} \frac{t^2}{m^2} \right) \right] \\
&= [e^{-2W}]_0 \prod_{i=x,y,z} \exp \left[-Q_i^2 \frac{h^2 \sqrt{V_0}}{8a^2} \frac{t^2}{m^2} \right] \\
&= [e^{-2W}]_0 \prod_{i=x,y,z} \exp \left[-\frac{\sqrt{V_0}}{2} \left(\frac{Q_i h}{2ma} \right)^2 t^2 \right] \\
&= [e^{-2W}]_0 \exp \left[-\frac{\sqrt{V_0}}{2} \left(\frac{|\mathbf{Q}| h}{2ma} \right)^2 t^2 \right]
\end{aligned} \tag{69}$$

We now define the time dependent correction factor

$$c(t) = \frac{[e^{-2W}]_t}{1 + \frac{s_0}{4\Delta^2}} \tag{70}$$

The measured intensity after time-of-flight t is

$$\frac{I_{\mathbf{Q}}(t)}{I_{\mathbf{Q}\infty}} = c(t)(S_{\mathbf{Q}} - 1) + 1 \tag{71}$$

2.2 Noise considerations

We want to consider the statistical fluctuations in the quantity S_Q due to the possibly random orientation of the spins. S_Q is defined as

$$S_Q = \frac{4}{N} \sum_{mn} e^{i\mathbf{Q} \cdot (\mathbf{R}_m - \mathbf{R}_n)} S_{zm} S_{zn} \quad (72)$$

Notice that this quantity can also be written as

$$S_Q = \frac{4}{N} \sum_m e^{i\mathbf{Q} \cdot \mathbf{R}_m} S_{zm} \sum_n e^{-i\mathbf{Q} \cdot \mathbf{R}_n} S_{zn} = \frac{4}{N} \left| \sum_m e^{i\mathbf{Q} \cdot \mathbf{R}_m} S_{zm} \right|^2 \quad (73)$$

In other words, S_Q can be written as the norm squared of a sum over the spin arrangement. When looking at the Bragg angle (that is when $\mathbf{Q} = (\pi, \pi, \pi)$) the exponential term in the sum can only take the values ± 1 , so the sum will be a real number. If the sample is not ordered, the distribution of the spins in the lattice is completely random and the sum can be represented as the total distance traveled in a random walk where the length of each step is $1/2$ and the probability of taking a step $+1/2$ is $p = 0.5$. When the sample has some order, the random walk will be biased, with $p > 0.5$ in general and $p = 1$ for a completely ordered sample.

To simplify matters let us take the factor of $1/2$ out of the spin variable and consider the random walk with unit step. We have then that

$$\sum_m e^{i\pi \cdot \mathbf{R}_m} S_{zm} = \frac{1}{2} X_N \quad (74)$$

where X_N is a random variable that represents the total distance traveled in a random walk with unit step after N steps. The probability density function for X_N is a binomial distribution

$$P(X_N = k) = \binom{N}{(N+k)/2} p^{(N+k)/2} (1-p)^{(N-k)/2} \quad (75)$$

which in the limit of a large number of steps can be approximated by a Gaussian probability distribution. Using $q = 1 - p$ this is

$$P(X_N = k) = \frac{1}{\sqrt{2\pi} \sqrt{4Npq}} \exp \left[-\frac{1}{2} \frac{(k - N(p-q))^2}{4Npq} \right] \quad (76)$$

The probability density function for X_N^2 can be obtained from $P(X_N = k)$ as

$$\begin{aligned} P(X_N^2 = y) &= \frac{1}{2\sqrt{y}} [P(X_N = \sqrt{y}) + P(X_N = -\sqrt{y})] \\ &= \frac{1}{2\sqrt{y}} \frac{1}{\sqrt{2\pi} \sqrt{4Npq}} \left(\exp \left[-\frac{1}{2} \frac{(\sqrt{y} - N(p-q))^2}{4Npq} \right] + \exp \left[-\frac{1}{2} \frac{(-\sqrt{y} - N(p-q))^2}{4Npq} \right] \right) \end{aligned} \quad (77)$$

where it needs to be kept in mind that $y \geq 0$.

We can go one step further and notice that since

$$S_\pi = \frac{X_N^2}{N} \quad (78)$$

the probability density function for S_π is

$$\begin{aligned} P(S_\pi = s) &= \frac{\sqrt{N}}{2\sqrt{s}} \left[P(X_N = \sqrt{sN}) + P(X_N = -\sqrt{sN}) \right] \\ &= \frac{\sqrt{N/s}}{2\sqrt{2\pi}\sqrt{4Npq}} \left(\exp \left[-\frac{1}{2} \frac{(\sqrt{sN} - N(p-q))^2}{4Npq} \right] + \exp \left[-\frac{1}{2} \frac{(-\sqrt{sN} - N(p-q))^2}{4Npq} \right] \right) \end{aligned} \quad (79)$$

The mean and variance of this probability density function can be calculated analytically by doing the integrals in Mathematica, the results are

$$\begin{aligned} \text{Mean}(S_\pi) &= N(2p-1)^2 + 4pq \\ \text{Var}(S_\pi) &= 16pq(N(2p-1)^2 + 2pq) \end{aligned} \quad (80)$$

For a completely random spin distribution we have $p = 1/2$ which gives $\overline{S_\pi} = 1$ and $\delta(S_\pi) = \sqrt{\text{Var}(S_\pi)} = \sqrt{2}$, which is independent of N . This variance is quite large, it is in fact larger than the mean value. In our experiment we take a number of shots n_s , where each shot is a measurement of S_π . If we happened to be looking at an unordered sample ($p = 0.5$), the uncertainty in the mean of S_π is then given by

$$\delta(\overline{S_\pi}) = \sqrt{2/n_s} \quad (81)$$

If we want this uncertainty to go to the 0.1 level we would need to average $n_s = 2/(0.1^2) = 200$ shots. We typically take some 10 shots, which for an unordered sample gives us $\delta(\overline{S_\pi}) = 0.44$.

2.2.1 Random realizations of S_π

We have run some numerical tests with sets of randomly ordered spins. The results from evaluating S_π numerically can be compared with the probability density function obtained in the previous section, this comparison is shown in Fig. 1.

2.2.2 Results for an AFM ordered core

We can also consider a sample which has an AFM ordered domain of size L_{AFM} at the center and then a randomly ordered shell on the outside. Care is taken to make sure the spin mixture is balanced. Numerically realizing random distributions of the spins in the shell we can obtain the distributions of S_π as a function of system size and size of the AFM domain. The results are shown in Fig. 2.

The mean values of the expected results at our detection cameras are shown for various values of N and L_{AFM} in Fig. 3.

By plotting the mean, standard deviation and their ratio for the quantity S_π we can see that the relative fluctuations only go down for values of S_π significantly larger than 1, which is a regime that would only be attained below the Neel transition. This is shown in Fig. 4.

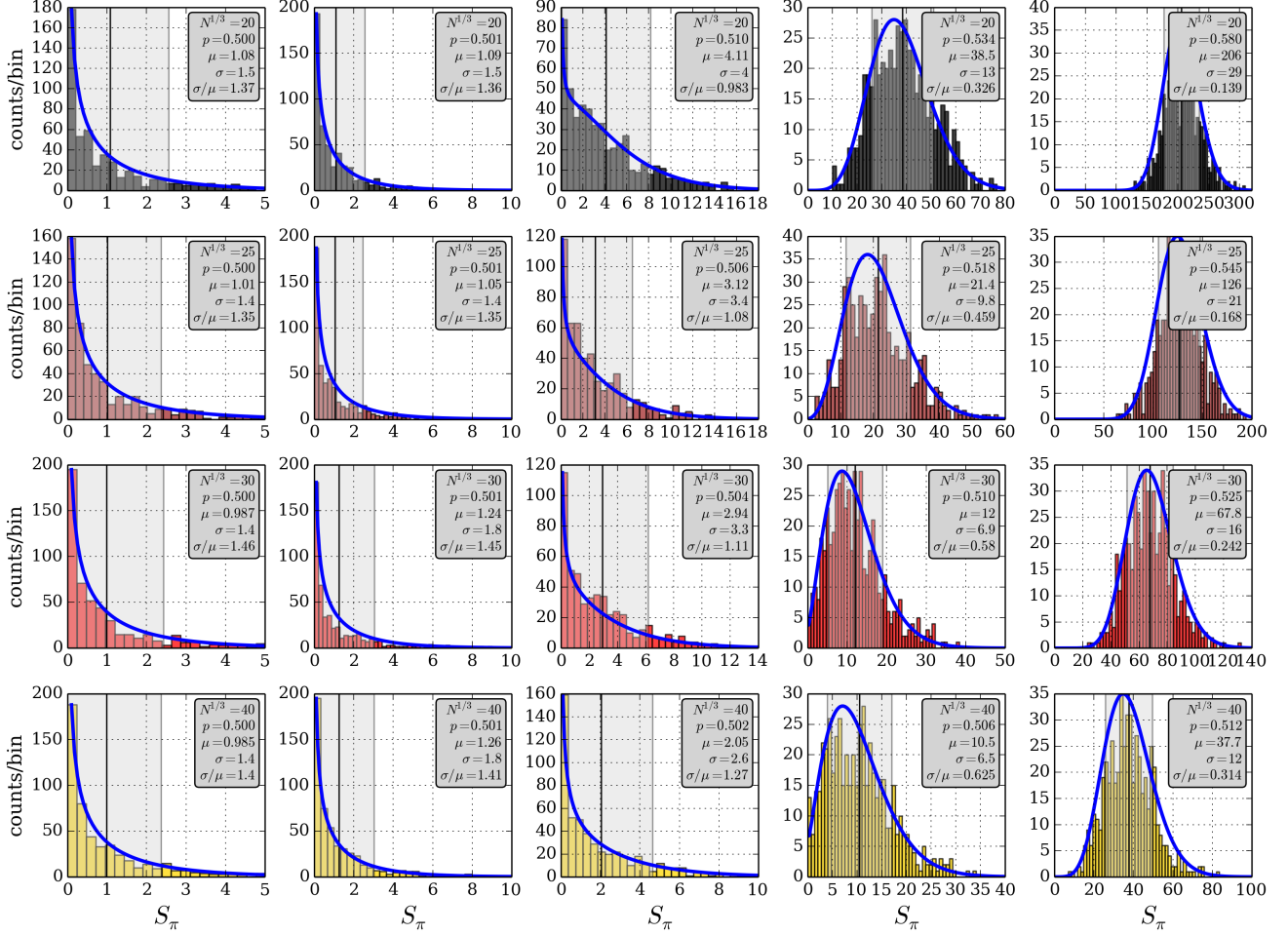


Figure 1: Distribution of S_π for randomly ordered spins. The spin ordering is parameterized by the parameter p as described in the text. The probability density function $P(S_\pi)$ as derived in the text is shown by the blue line. The thin black line denotes the mean of the distribution and the shaded gray area denotes ± 1 standard deviations.

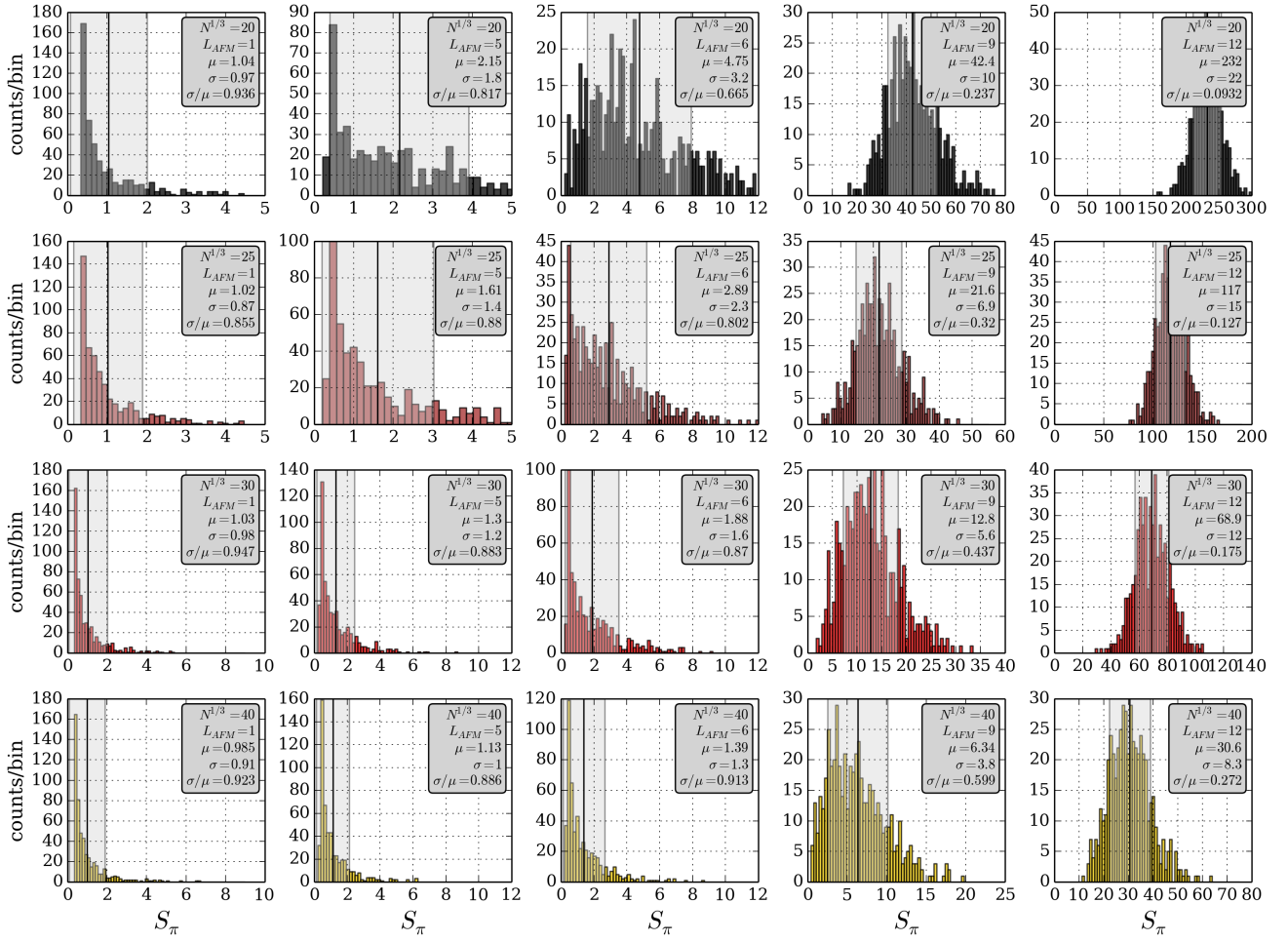


Figure 2: Distribution of S_π for randomly ordered spins. The spin ordering is parameterized by the size of the AFM domain as described in the text. The thin black line denotes the mean and the shaded gray area denotes ± 1 standard deviations.

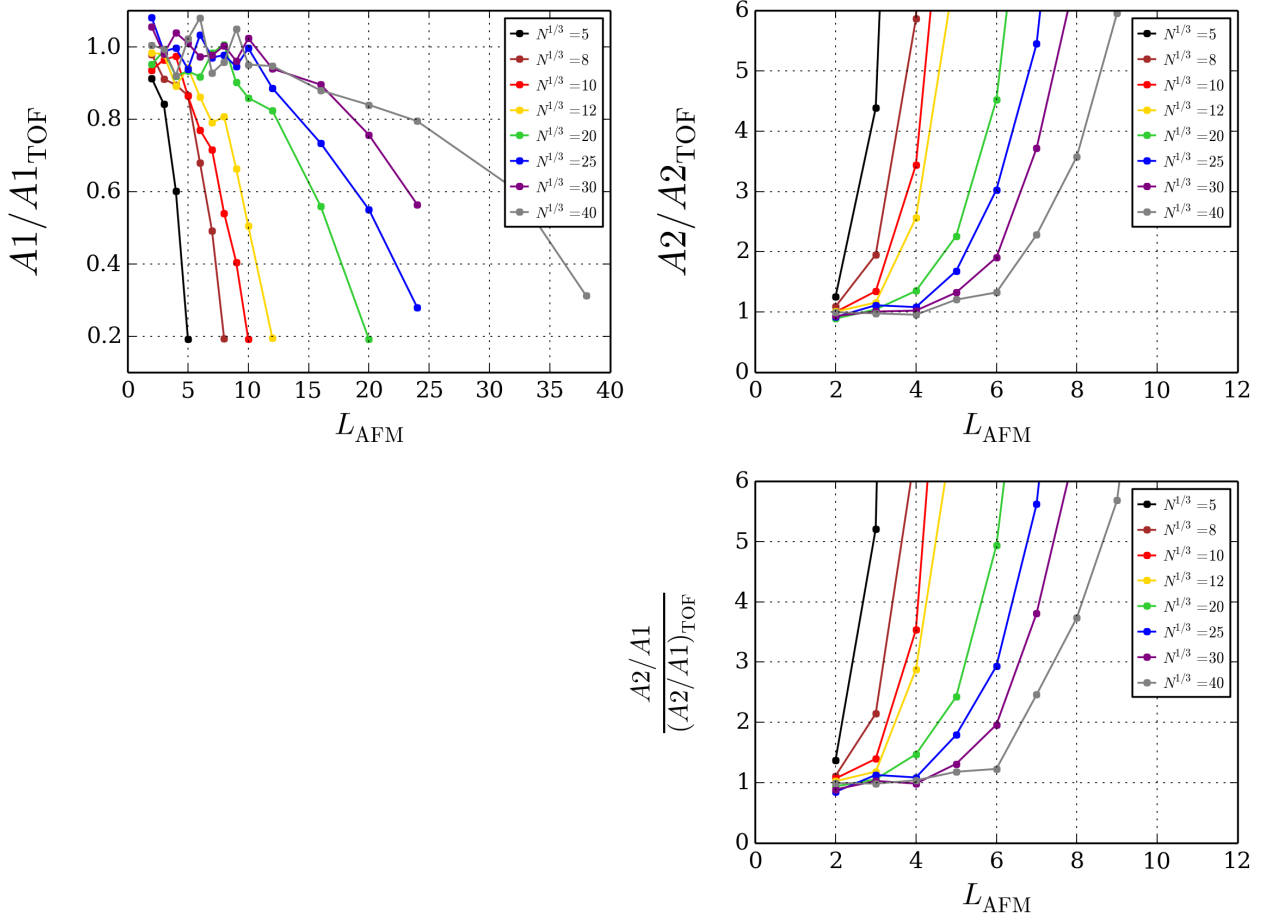


Figure 3: Mean value of S_π for randomly ordered spins. The spin ordering is parameterized by the size of the AFM domain as described in the text.

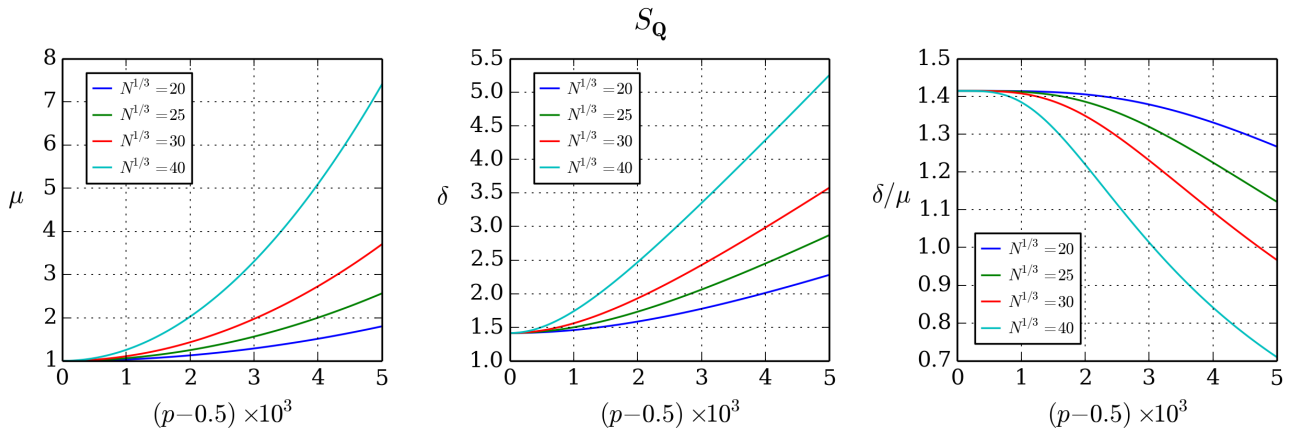


Figure 4: Mean value, variance, and their ratio for S_π are plotted for different values of p , and N .

2.3 Angular dependence of S_Q

In this section we wish to obtain the analytical dependence of the spin structure factor S_Q as a function of \mathbf{Q} . We assume that the spin-spin correlation function has a correlation length L_c , so we can write

$$\langle S_{zm} S_{zn} \rangle = \frac{1}{4} e^{-i\pi(\mathbf{R}_m - \mathbf{R}_n)} e^{-|\mathbf{R}_m - \mathbf{R}_n|/L_c} \quad (82)$$

Here $\boldsymbol{\pi} = \frac{2\pi}{a}(1/2, 1/2, 1/2)$ ensures that the spins are antiferromagnetically ordered and their correlation decays over a length L_c .

Our goal is to obtain the spin structure factor, which is defined as

$$\begin{aligned} S_Q &= \frac{4}{N} \sum_{mn} e^{i\mathbf{Q}(\mathbf{R}_m - \mathbf{R}_n)} \langle S_{zm} S_{zn} \rangle = \frac{4}{N} \sum_{mn} e^{i\mathbf{Q}(\mathbf{R}_m - \mathbf{R}_n)} \frac{1}{4} e^{-i\pi(\mathbf{R}_m - \mathbf{R}_n)} e^{-|\mathbf{R}_m - \mathbf{R}_n|/L_c} \\ &= \frac{1}{N} \sum_{mn} e^{i(\mathbf{Q} - \boldsymbol{\pi})(\mathbf{R}_m - \mathbf{R}_n)} e^{-|\mathbf{R}_m - \mathbf{R}_n|/L_c} \end{aligned} \quad (83)$$

We introduce the vector $\mathbf{p} = \mathbf{Q} - \boldsymbol{\pi}$ and split the sum into $m = n$ and $m \neq n$ parts:

$$\begin{aligned} S_Q &= \frac{1}{N} \left(\sum_{m=n} + \sum_{m \neq n} \right) e^{i\mathbf{p}(\mathbf{R}_m - \mathbf{R}_n)} e^{-|\mathbf{R}_m - \mathbf{R}_n|/L_c} \\ &= 1 + \sum_{m \neq n} e^{i\mathbf{p}(\mathbf{R}_m - \mathbf{R}_n)} e^{-|\mathbf{R}_m - \mathbf{R}_n|/L_c} \end{aligned} \quad (84)$$

We change one of the indices in the sum according to $\mathbf{R}_m = \mathbf{R}_n + \mathbf{R}_k$, which gives

$$S_Q = 1 + \frac{1}{N} \sum_n \sum_{k \neq 0} e^{i\mathbf{p}\mathbf{R}_k} e^{-|\mathbf{R}_k|/L_c} = 1 + \sum_{k \neq 0} e^{i\mathbf{p}\mathbf{R}_k} e^{-|\mathbf{R}_k|/L_c} \quad (85)$$

Notice that on the second step above we have carried out the sum over n , assuming that the crystal is sufficiently large such that there are no edge effects associated with the translation that was performed upon changing the index variables. This is a valid assumption as long as the correlation length, L_c is significantly smaller than the size of the entire crystal.

We will now approximate the sum over k with an integral, $\sum_{k \neq 0} \rightarrow a^{-3} \int_{\mathbb{R}^3} d^3\mathbb{R}$, where a is the lattice spacing.

$$S_Q = 1 + \sum_{k \neq 0} e^{i\mathbf{p}\mathbf{R}_k} e^{-|\mathbf{R}_k|/L_c} = 1 + \frac{1}{a^3} \int_{\mathbb{R}^3} d^3\mathbb{R} e^{i\mathbf{p}\mathbf{R}_k} e^{-|\mathbf{R}_k|/L_c} \quad (86)$$

The integral that remains is the 3D Fourier transform of a spherically symmetric function. We will show below that this can be replaced by the Fourier-Bessel transform of the radial function e^{-R/L_c} .

Let's look at the Fourier transform $F(\mathbf{p})$ of a spherically symmetric function $f(R)$, choosing the polar axis to be along \mathbf{p} :

$$F(\mathbf{p}) = \int_{\mathbb{R}^3} d^3\mathbb{R} e^{i\mathbf{p}\mathbf{R}} f(R) = \int_0^\infty \int_0^\pi \int_0^{2\pi} e^{ipR \cos \theta} f(R) R^2 dR \sin \theta d\theta d\phi \quad (87)$$

We will replace θ according to $x = \cos \theta$, $dx = \sin \theta d\theta$.

$$\begin{aligned} F(p) &= 2\pi \int_0^\infty f(R) R^2 \left[\int_{-1}^1 e^{ipRx} dx \right] dR = 2\pi \int_0^\infty f(R) R^2 \left[\frac{e^{ipR} - e^{-ipR}}{ipR} \right] dR \\ &= 4\pi \int_0^\infty f(R) \frac{\sin(pR)}{pR} R^2 dR \end{aligned} \quad (88)$$

This last expression is the Fourier-Bessel transform of $f(R)$.

Applying this result to the integral in the definition of the structure factor, we have

$$S_Q = 1 + \frac{4\pi}{a^3} \int_0^\infty e^{-R/L_c} \frac{\sin(pR)}{pR} R^2 dR \quad (89)$$

This last integral can be plugged into Mathematica to obtain

$$S_Q - 1 = \frac{8\pi}{a^3} \frac{L_c^3}{[1 + (L_c|\mathbf{Q} - \boldsymbol{\pi}|)^2]^2} \quad (90)$$

We want to obtain the angular dependence of S_Q when changing the input angle of the probe light used for Bragg scattering. Suppose the vectors $\mathbf{k}_{\text{in}0}$ and $\mathbf{k}_{\text{out}0}$ satisfy the Bragg condition, such that

$$\mathbf{k}_{\text{in}0} - \mathbf{k}_{\text{out}0} = \boldsymbol{\pi} \quad (91)$$

If we rotate the input direction slightly by an angle α , then

$$\mathbf{k}_{\text{in}} = \mathbf{k}_{\text{in}0} + |\mathbf{k}_{\text{in}0}| \alpha \hat{\mathbf{n}}_0 \quad (92)$$

where $\hat{\mathbf{n}}_0$ is a unit vector perpendicular to $\mathbf{k}_{\text{in}0}$. We then have that

$$p = |\mathbf{Q} - \boldsymbol{\pi}| = |\mathbf{k}_{\text{in}} - \mathbf{k}_{\text{out}0} - \boldsymbol{\pi}| = |\mathbf{k}_{\text{in}0} + |\mathbf{k}_{\text{in}0}| \alpha \hat{\mathbf{n}}_0 - \mathbf{k}_{\text{out}0} - \boldsymbol{\pi}| = |\mathbf{k}_{\text{in}0}| \alpha = \frac{2\pi}{\lambda_B} \alpha \quad (93)$$

where λ_B is the wavelength of the Bragg probe.

We then have that for a small angular change α in the input Bragg probe

$$S(\alpha) - 1 = 8\pi \frac{(L_c/a)^3}{\left[1 + \left(\frac{2\pi L_c}{\lambda_B} \alpha \right)^2 \right]^2} \quad (94)$$

or

$$\frac{S(\alpha) - 1}{S_\pi} = \frac{1}{\left[1 + \left(\frac{2\pi L_c}{\lambda_B} \alpha \right)^2 \right]^2} \approx \exp \left[-2 \left(\frac{2\pi}{\lambda_B} L_c \alpha \right)^2 \right] \quad (95)$$

We see that the $1/e$ radius of the angular profile is given by

$$\alpha_{1/e} = \frac{\lambda_B}{2\pi\sqrt{2}} \frac{1}{L_c} = \frac{\lambda_B/a}{2\pi\sqrt{2}} \frac{1}{L_c/a} = \frac{0.14}{L_c/a} \quad (96)$$

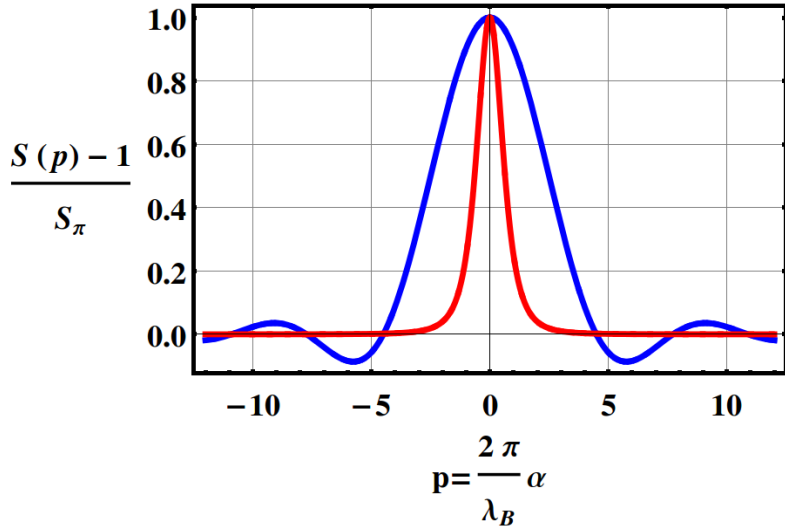


Figure 5: Angular variation of S_Q as a function of $p = \frac{2\pi\lambda_B}{\alpha}$ where α is a small angular deviation of the input Bragg beam. The blue line is for the box correlation function and the red line is for the exponential decay correlation.

Alternately we can consider a spin-spin correlation function that is shaped like a box of length L_{AFM} :

$$\langle S_{zm} S_{zn} \rangle = \begin{cases} \frac{1}{4} & \text{if } |\mathbf{R}_m - \mathbf{R}_n| \leq L_{\text{AFM}} \\ 0 & \text{if } |\mathbf{R}_m - \mathbf{R}_n| > L_{\text{AFM}} \end{cases} \quad (97)$$

In this case we find that

$$\begin{aligned} S_Q &= 1 + \frac{4\pi}{a^3} \int_0^{L_{\text{AFM}}} \frac{\sin(pr)}{pr} R^2 dR \\ &= 1 + \frac{4\pi}{a^3} \left[\frac{\sin(pL_{\text{AFM}}) - pL_{\text{AFM}} \cos(pL_{\text{AFM}})}{p^3} \right] \end{aligned} \quad (98)$$

$$\begin{aligned} \frac{S(\alpha) - 1}{S_\pi} &= \frac{3}{L_{\text{AFM}}^3} \frac{\sin\left(\frac{2\pi L_{\text{AFM}}}{\lambda_B} \alpha\right) - \frac{2\pi\alpha}{\lambda_B} L_{\text{AFM}} \cos\left(\frac{2\pi L_{\text{AFM}}}{\lambda_B} \alpha\right)}{p^3} \\ &\approx \exp\left[-\frac{1}{10} \left(\frac{2\pi}{\lambda_B} L_c \alpha\right)^2\right] \end{aligned} \quad (99)$$

In this case the $1/e$ radius of the angular profile is given by

$$\alpha_{1/e} = \frac{\lambda_B}{2\pi} \sqrt{10} \frac{1}{L_c} = \frac{\lambda_B/a}{2\pi} \sqrt{10} \frac{1}{L_c/a} = \frac{0.634}{L_c/a} \quad (100)$$

The $1/e$ radii obtained for an exponentially decaying correlation and for a correlation function that looks like a box differ by a factor of $634/140 = 4.52$ which is somewhat unexpected. A comparison of the two angular functions is shown in Fig. 5.

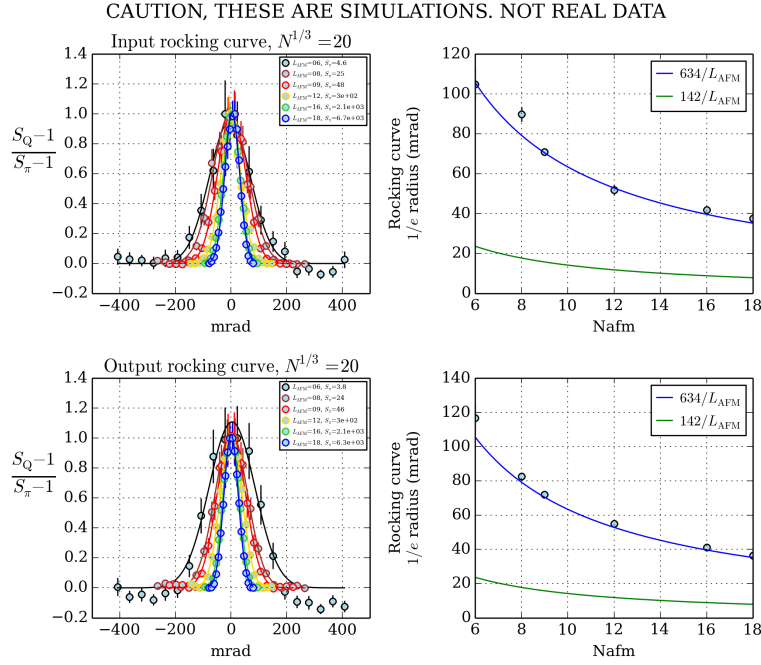


Figure 6: Rocking curve for $N^{1/3}=20$. The blue line is the analytical result for the box function correlations and the green line is the analytical result for the exponentially decaying correlations.

2.3.1 Angular dependence of S_Q for a matrix of randomly ordered spins

We have performed simulations of Bragg scattering on a 3D lattice of randomly ordered spins. The lattice has an AFM ordered core with size L_{AFM} at the center and a randomly ordered shell on the outside. The total number of spins in the lattice is N , and the lattice is a cube with side equal to $N^{1/3}$.

Below we will plot the results of varying the angle of incidence of the probe Bragg beam, by a small amount around the value that satisfy the Bragg condition. We also show the results of varying the observation angle slightly away from the angle that satisfies the Bragg condition. These two variations are referred to as input rocking curve and output rocking curve respectively.

We show plots of the input and output rocking curve, and the $1/e$ radii of the angular distributions as a function of the AFM core size. We do this for crystal sizes of $N^{1/3} = 20, 30, 40, 50$, as shown if Figs. 6-9.

2.3.2 Remarks about angular distribution

We see that the numerical simulations using a random matrix with an AFM core agree well with the analytical calculation, which involves taking the 3D Fourier transform of a box function. The main approximation done in the analytical calculation was the replacement of the sum over particles with the integral over all of space. Taking the integral over all of space neglects anything that is happening at the edge of the system. This is fine for correlation functions that have a finite support, such as the box or the exponentially decaying function. If the system had long range order then an integral over all of space would diverge.

It is surprising that the $1/e$ radius of the angular distribution can be so different for the two different correlation functions studied. They differ by a factor of 4.

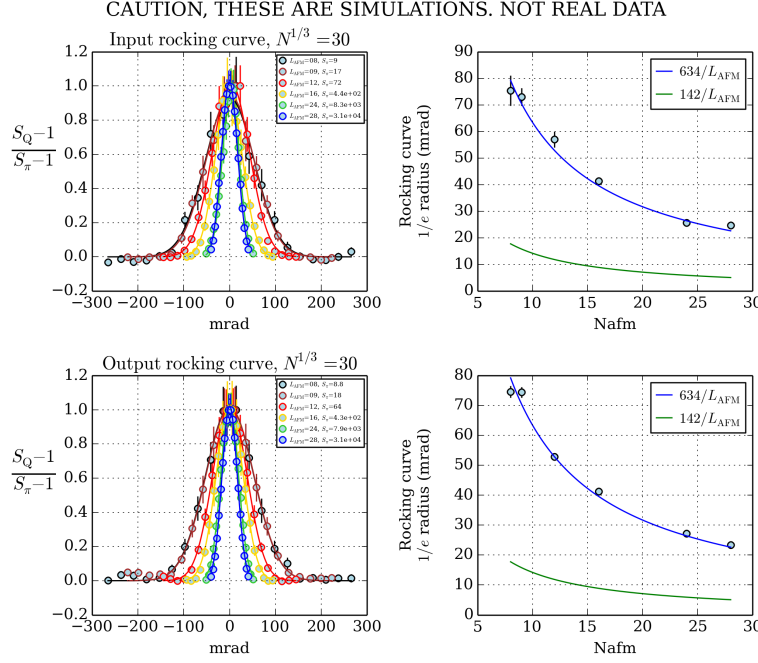


Figure 7: Rocking curve for $N^{1/3}=30$. The blue line is the analytical result for the box function correlations and the green line is the analytical result for the exponentially decaying correlations.

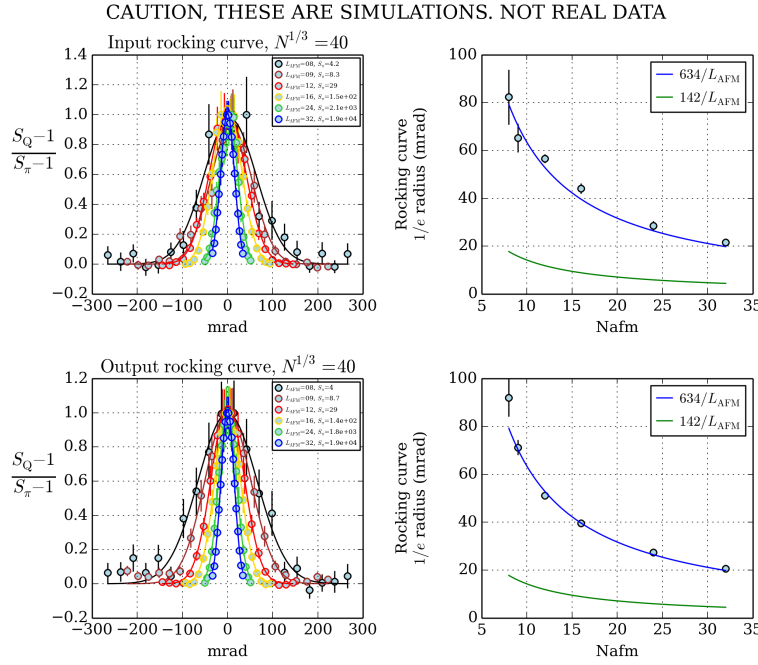


Figure 8: Rocking curve for $N^{1/3}=40$. The blue line is the analytical result for the box function correlations and the green line is the analytical result for the exponentially decaying correlations.

CAUTION, THESE ARE SIMULATIONS. NOT REAL DATA

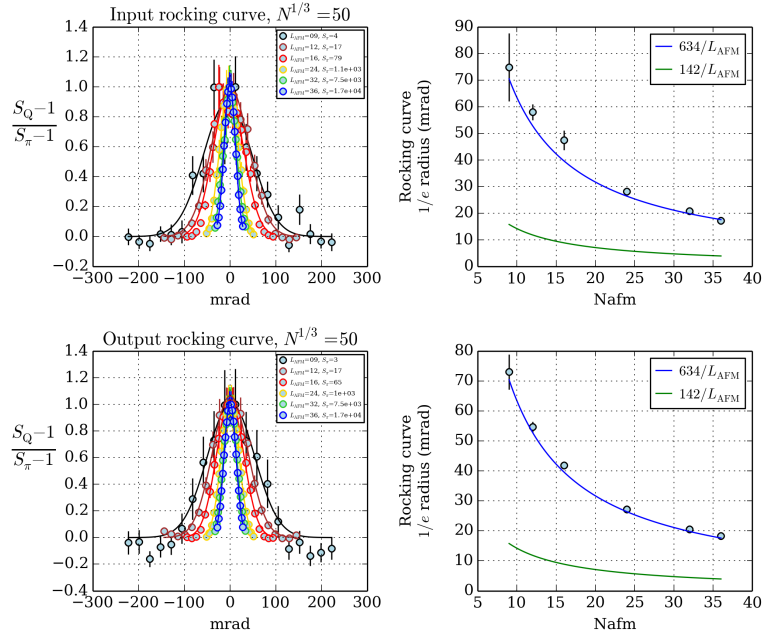


Figure 9: Rocking curve for $N^{1/3}=50$. The blue line is the analytical result for the box function correlations and the green line is the analytical result for the exponentially decaying correlations.

2.4 Magneto-association and contributions from doubly occupied sites

In our experiment we have the possibility to magneto-associate (MA) the atoms in doubly occupied sites prior to a measurement of the scattered light. The formed molecules are largely detuned from the probe light and the light that they scatter is negligible. In this section we study the implications of MA for the comparison between experimental measurements and the structure factor as calculated by the theorists.

We start from Eq. 55 and will separate the sums over atoms in singly and doubly occupied sites. Without carrying out the sums, Eq. 55 reads

$$I_{\mathbf{Q}} = \frac{I_{\mathbf{Q}\infty}}{N} \left[4c \sum_{mn} e^{i\mathbf{Q}(\mathbf{R}_m - \mathbf{R}_n)} S_{zm} S_{zn} - c \sum_n + \sum_n \right] \quad (101)$$

With MA prior to the intensity measurement, there is no contribution to the scattered light from atoms in doubly occupied sites, so denoting as \mathcal{S} the set of singly occupied sites, we have

$$\begin{aligned} I_{\mathbf{Q}_{\text{MA}}} &= \frac{I_{\mathbf{Q}\infty}}{N} \left[4c \sum_{m \in \mathcal{S}} e^{i\mathbf{Q}\mathbf{R}_m} S_{zm} \sum_{n \in \mathcal{S}} e^{-i\mathbf{Q}\mathbf{R}_n} S_{zn} - c \sum_{n \in \mathcal{S}} + \sum_{n \in \mathcal{S}} \right] \\ &= \frac{I_{\mathbf{Q}\infty}}{N} \left[4c \sum_{m \in \mathcal{S}} e^{i\mathbf{Q}\mathbf{R}_m} S_{zm} \sum_{n \in \mathcal{S}} e^{-i\mathbf{Q}\mathbf{R}_n} S_{zn} - cN(1-D) + N(1-D) \right] \end{aligned} \quad (102)$$

where D is the fraction of atoms in doubly occupied sites.

Denoting the set of atoms in doubly occupied sites as \mathcal{D} , we point out that

$$\sum_{m \in \mathcal{D}} e^{\pm i\mathbf{Q}\mathbf{R}_m} S_{AM} = 0 \quad (103)$$

since the contributions cancel out in pairs as $e^{\pm i\mathbf{Q}\mathbf{R}_m} (+1/2 - 1/2) = 0$. This allows us to remove the $\in \mathcal{S}$ constraint in the remaining sums:

$$\sum_{m \in \mathcal{S}} e^{\pm i\mathbf{Q}\mathbf{R}_m} S_{zm} = \sum_m e^{\pm i\mathbf{Q}\mathbf{R}_m} S_{zm} \quad (104)$$

and obtain for the intensity after MA

$$\begin{aligned} I_{\mathbf{Q}_{\text{MA}}} &= \frac{I_{\mathbf{Q}\infty}}{N} \left[4c \sum_m e^{i\mathbf{Q}\mathbf{R}_m} S_{zm} \sum_n e^{-i\mathbf{Q}\mathbf{R}_n} S_{zn} - cN(1-D) + N(1-D) \right] \\ &= I_{\mathbf{Q}\infty} [cS_{\mathbf{Q}} - c(1-D) + (1-D)] \end{aligned} \quad (105)$$

We introduce the simplifying notation

$$\frac{I_{\mathbf{Q}_{\text{MA}}}}{I_{\mathbf{Q}\infty}} \equiv i_{\mathbf{Q}_{\text{MA}}} \quad (106)$$

and solve for the spin structure factor to obtain

$$S_{\mathbf{Q}} = \frac{1}{c} (i_{\mathbf{Q}_{\text{MA}}} - 1) + 1 + \frac{D}{c} (1 - c) \quad (107)$$

To measure the fraction of atoms in doubly occupied sites, D , we can make a measurement of the

scattered intensity after MA and a large TOF. Combined with the TOF measurement without MA we have

$$D = 1 - \frac{I_{Q_{MA\infty}}}{I_{Q\infty}} \equiv 1 - i_S \quad (108)$$

giving finally

$$S_Q = \frac{i_{Q_{MA}}}{c} + \frac{c-1}{c} i_S \quad (109)$$

We have taken sets of data where we only record $I_{Q_{MA\infty}}$ and $I_{Q_{MA}}$. Under this conditions we can use the following two equations to solve for the structure factor

$$\frac{I_{Q_{MA}}}{I_{Q\infty}} = c S_Q - c(1-D) + (1-D) \quad \frac{I_{Q_{MA\infty}}}{I_{Q\infty}} = 1 - D \quad (110)$$

$$S_Q = \frac{1-D}{c} (j_{Q_{MA}} + c-1) \quad j_{Q_{MA}} \equiv \frac{I_{Q_{MA}}}{I_{Q_{MA\infty}}} \quad (111)$$

We still need knowledge of the double occupancy D , so for sets with only $I_{Q_{MA\infty}}$ and $I_{Q_{MA}}$ we have to use D from another data set.

2.5 Data at short time-of-flight

In the above section we considered $I_{Q\infty}$, a measurement of the intensity with a time-of-flight long enough such that the Debye-Waller factor $e^{-2W} \rightarrow 0$. For some of the data we have taken, the TOF is $6 \mu s$, which in some cases is not long enough for the Debye-Waller factor be negligible. In this section we look at the determination of S_Q with time of flight data for which one cannot assume $e^{-2W} \rightarrow 0$.

We recall that the Debye-Waller factor is defined as

$$e^{-2W} = \prod_{i=x,y,z} e^{-Q_i^2 \langle r_i^2 \rangle} \quad (112)$$

where Q_i is the i^{th} component of the momentum transfer $\mathbf{Q} = \mathbf{k}' - \mathbf{k}$, with \mathbf{k}' and \mathbf{k} the wave vectors of the outgoing and incoming light respectively. The time-of-flight dependence of the Debye-Waller factor is through the expanding size of the atomic wavefunctions. For an in-situ picture $\langle r_i^2 \rangle$ corresponds to the position spread of the lattice site's harmonic oscillator ground state. After the atoms are released from the lattice the spread of the wavefunction satisfies

$$\begin{aligned} \langle r_i^2 \rangle_t &= \langle r_i^2 \rangle_0 + \frac{t^2}{m^2} \langle p_i^2 \rangle_0 \\ &= \langle r_i^2 \rangle_0 + \frac{t^2}{m^2} \frac{\hbar^2}{4 \langle r_i^2 \rangle_0} \end{aligned} \quad (113)$$

In a harmonic oscillator potential we have

$$\langle r^2 \rangle = \frac{\hbar}{2m\omega} \quad (114)$$

and since in a lattice of depth V_0 recoils, $\hbar\omega = 2E_R\sqrt{V_0}$

$$\langle r^2 \rangle = \frac{a^2}{2\pi^2\sqrt{V_0}} \quad (115)$$

where a is the lattice spacing.

We then have for the Debye-Waller factor as a function of time-of-flight

$$\begin{aligned}
[e^{-2W}]_t &= \prod_{i=x,y,z} \exp \left[-Q_i^2 \left(\frac{a^2}{2\pi^2\sqrt{V_0}} + \frac{h^2\sqrt{V_0}}{8a^2} \frac{t^2}{m^2} \right) \right] \\
&=[e^{-2W}]_0 \prod_{i=x,y,z} \exp \left[-Q_i^2 \frac{h^2\sqrt{V_0}}{8a^2} \frac{t^2}{m^2} \right] \\
&=[e^{-2W}]_0 \prod_{i=x,y,z} \exp \left[-\frac{\sqrt{V_0}}{2} \left(\frac{Q_i h}{2ma} \right)^2 t^2 \right] \\
&=[e^{-2W}]_0 \exp \left[-\frac{\sqrt{V_0}}{2} \left(\frac{|\mathbf{Q}|h}{2ma} \right)^2 t^2 \right]
\end{aligned} \tag{116}$$

We now define the time dependent correction factor

$$c(t) = \frac{[e^{-2W}]_t 4\Delta^2}{4\Delta^2 + 2I_p/I_{\text{sat}}} \tag{117}$$

The measured intensity after time-of-flight t is

$$\frac{I_{\mathbf{Q}}(t)}{I_{\mathbf{Q}\infty}} = c(t)(S_{\mathbf{Q}} - 1) + 1 \tag{118}$$

Consider two measurements, one at $t = 0$, the other one at $t = T$,

$$\frac{I_{\mathbf{Q}}(t=0)}{I_{\mathbf{Q}\infty}} = c(0)(S_{\mathbf{Q}} - 1) + 1 \quad \frac{I_{\mathbf{Q}}(t=T)}{I_{\mathbf{Q}\infty}} = c(T)(S_{\mathbf{Q}} - 1) + 1 \tag{119}$$

Their ratio is

$$\frac{I_{\mathbf{Q}}(t=0)}{I_{\mathbf{Q}}(t=T)} = \frac{c(0)(S_{\mathbf{Q}} - 1) + 1}{c(T)(S_{\mathbf{Q}} - 1) + 1} \equiv i_{\mathbf{Q}_T} \tag{120}$$

which can be solved to give

$$S_{\mathbf{Q}} = \frac{1 - c(0) - i_{\mathbf{Q}_T}(1 - c(T))}{i_{\mathbf{Q}_T}c(T) - c(0)} \tag{121}$$

2.6 Simultaneous measurement of the structure factor for two different values of \mathbf{Q}

In the sections above we have shown how to measure the spin structure factor $S_{\mathbf{Q}}$ by measuring the scattered intensity in-situ and after time-of-flight. An issue that arises with this measurement is that the in-situ and TOF measurements require two different realizations of the experiment.

In our setup we have the possibility of measuring the scattered intensity at two different output angles. One of the angles corresponds to a momentum transfer $\mathbf{Q} = \frac{2\pi}{a}(\frac{1}{2}, \frac{1}{2}, \frac{1}{2}) \equiv \boldsymbol{\pi}$, which offers the possibility of measuring the staggered magnetization of the system, i.e. the degree of antiferromagnetic ordering. The other angle corresponds to a momentum transfer $\mathbf{Q} = \frac{2\pi}{a}(0.4, -0.1, -0.04) \equiv \boldsymbol{\theta}$. The structure factor can also be measured at this value of \mathbf{Q} and compared with theoretical calculations. Since this momentum transfer does not measure the staggered magnetization it may be used as a normalization for the measurement at $\mathbf{Q} = \boldsymbol{\pi}$.

For the measurements at $\boldsymbol{\pi}$ and $\boldsymbol{\theta}$ we have (without magneto-association)

$$S_{\boldsymbol{\pi}} = (i_{\boldsymbol{\pi}} - 1 + c_{\boldsymbol{\pi}})/c_{\boldsymbol{\pi}} \quad S_{\boldsymbol{\theta}} = (i_{\boldsymbol{\theta}} - 1 + c_{\boldsymbol{\theta}})/c_{\boldsymbol{\theta}} \quad (122)$$

$$\frac{S_{\boldsymbol{\pi}}}{S_{\boldsymbol{\theta}}} = \frac{i_{\boldsymbol{\pi}} - 1 + c_{\boldsymbol{\pi}}}{i_{\boldsymbol{\theta}} - 1 + c_{\boldsymbol{\theta}}} \left(\frac{c_{\boldsymbol{\theta}}}{c_{\boldsymbol{\pi}}} \right) \quad (123)$$

To make use of the simultaneous measurement of I at $\boldsymbol{Q} = \boldsymbol{\pi}, \boldsymbol{\theta}$ we define

$$\left(\frac{I_{\boldsymbol{\pi}}}{I_{\boldsymbol{\theta}}} \right) \Big/ \left(\frac{I_{\boldsymbol{\pi}\infty}}{I_{\boldsymbol{\theta}\infty}} \right) \equiv i_{\boldsymbol{\pi}/\boldsymbol{\theta}} \quad (124)$$

The advantage here is that the ratio $\frac{I_{\boldsymbol{\pi}\infty}}{I_{\boldsymbol{\theta}\infty}}$ is determined only by the solid angle and responsivity of the cameras. One can calibrate this ratio beforehand and then, using the calibration, get a single shot measurement of $i_{\boldsymbol{\pi}/\boldsymbol{\theta}}$

The ratio of the structure factors at $\boldsymbol{\pi}$ and $\boldsymbol{\theta}$ is given by

$$\frac{S_{\boldsymbol{\pi}}}{S_{\boldsymbol{\theta}}} = \frac{i_{\boldsymbol{\pi}/\boldsymbol{\theta}} - (1 - c_{\boldsymbol{\pi}})/i_{\boldsymbol{\theta}}}{1 - (1 - c_{\boldsymbol{\theta}})/i_{\boldsymbol{\theta}}} \left(\frac{c_{\boldsymbol{\theta}}}{c_{\boldsymbol{\pi}}} \right) \quad (125)$$

If our correction factors were close to 1 we could obtain the ratio of structure factors in one shot as

$$\frac{S_{\boldsymbol{\pi}}}{S_{\boldsymbol{\theta}}} \approx i_{\boldsymbol{\pi}/\boldsymbol{\theta}} \quad (126)$$

Besides being able to get this in one shot it has the added advantage that any common mode noise between the two cameras gets canceled out, this includes atom number fluctuations and fluctuations in the intensity or polarization of the probe light. Unfortunately with our $50 E_R$ lattice and $I_p/I_{\text{sat}} = 15$ we have

$$c_{\boldsymbol{\pi}} = 0.686 \quad c_{\boldsymbol{\theta}} = 0.805 \quad (127)$$

which results in a non-negligible correction that depend on $i_{\boldsymbol{\theta}}$. In our case this is not such a drawback because the camera located at $\boldsymbol{\theta}$ has a solid angle that is 10 time larger than the camera located at $\boldsymbol{\pi}$.

We can also obtain formulas for the ratio $S_{\boldsymbol{\pi}}/S_{\boldsymbol{\theta}}$ under the conditions described in the two previous sections.

In the case where the time-of-flight is not large enough for $e^{-2W} \rightarrow 0$ we have the formula

$$\frac{S_{\boldsymbol{\pi}}}{S_{\boldsymbol{\theta}}} = \frac{[1 - c_{\boldsymbol{\pi}}(0)]/i_{\boldsymbol{\theta}_T} - i_{(\boldsymbol{\pi}/\boldsymbol{\theta})_T}[1 - c_{\boldsymbol{\pi}}(T)]}{[1 - c_{\boldsymbol{\theta}}(0)]/i_{\boldsymbol{\theta}_T} - [1 - c_{\boldsymbol{\theta}}(T)]} \frac{c_{\boldsymbol{\theta}}(T) - c_{\boldsymbol{\theta}}(0)/i_{\boldsymbol{\theta}_T}}{i_{(\boldsymbol{\pi}/\boldsymbol{\theta})_T} c_{\boldsymbol{\pi}}(T) - c_{\boldsymbol{\pi}}(0)/i_{\boldsymbol{\theta}_T}} \quad (128)$$

If the in-situ intensity is measured after magneto-association we have

$$\frac{S_{\boldsymbol{\pi}}}{S_{\boldsymbol{\theta}}} = \frac{c_{\boldsymbol{\theta}}}{c_{\boldsymbol{\pi}}} \frac{i_{(\boldsymbol{\pi}/\boldsymbol{\theta})_{\text{MA}}} + (c_{\boldsymbol{\pi}} - 1)(1 - D)/i_{\boldsymbol{\theta}_{\text{MA}}}}{1 + (c_{\boldsymbol{\theta}} - 1)(1 - D)/i_{\boldsymbol{\theta}_{\text{MA}}}} \quad (129)$$

If both the in-situ and TOF intensity are measured after magneto-association we have

$$\frac{S_{\boldsymbol{\pi}}}{S_{\boldsymbol{\theta}}} = \frac{c_{\boldsymbol{\theta}}}{c_{\boldsymbol{\pi}}} \frac{j_{(\boldsymbol{\pi}/\boldsymbol{\theta})_{\text{MA}}} + (c_{\boldsymbol{\pi}} - 1)/j_{\boldsymbol{\theta}_{\text{MA}}}}{1 + (c_{\boldsymbol{\theta}} - 1)j_{\boldsymbol{\theta}_{\text{MA}}}} \quad (130)$$

2.7 Summary of structure factor formulas

Below we show the different ways to calculate the structure factor from our measurements. A correction factor, c_Q appears in the formulas to account for the non-unity Debye-Waller factor in the lattice and also for the intensity of the probe beam. The formula for the correction factor is

$$c_Q = \frac{e^{-2W} 4\Delta^2}{(4\Delta^2 + 2I_p/I_{\text{sat}})} \quad (131)$$

The Debye-Waller factor, e^{-2W} depends on the momentum transfer \mathbf{Q} . In our experiment the corrections are significant. The largest lattice depth we can reach is $50 E_R$, and in order to moderately overcome the dark noise of the camera we use a probe intensity of $I_p = 15 I_{\text{sat}}$. This results in the following values for π and θ , the two values of the momentum transfer that we have access to:

$$\pi = \frac{2\pi}{a}(0.5, 0.5, 0.5) \quad \theta = \frac{2\pi}{a}(0.4, -0.1, -0.04) \quad (132)$$

$$e_{\pi}^{-2W} = 0.81 \quad e_{\theta}^{-2W} = 0.95 \quad 1 + \frac{I_p/I_{\text{sat}}}{2\Delta^2} = 1.18 \quad (133)$$

$$c_{\pi} = 0.686 \quad c_{\theta} = 0.805 \quad (134)$$

The duration of our scattering pulse is $1.7 \mu\text{s}$, and we scatter on the average 4.7 photons per atom. At our lattice depth of $50 E_R$, the square of the Lamb-Dicke parameter is $\eta_{LD}^2 = 0.07$ which means that we can approximately scatter 14 photons per atom before we kick the atom into an excited band. At the moment we have not introduced corrections for atoms recoiling into excited bands during the measurement.

In the latest data that we have taken at $5.5 E_R$ as a function of U/t , we always do a magneto-association sweep before the in-situ picture. We also take time-of-flight pictures with and without magneto-association. The following table lists the quantities that we measure

CCD measurements:

$I_{Q_{\text{MA}}}$	In-situ intensity measured at momentum transfer \mathbf{Q} after magneto-association of doubly occupied sites into molecules. Molecules are dark to the probe light.
$I_{Q_{\infty}}$	Time-of-flight intensity measured at momentum transfer \mathbf{Q} . We use $\text{TOF} = 10 \mu\text{s}$.
$I_{Q_{\text{MA}\infty}}$	Time-of-flight intensity measured at momentum transfer \mathbf{Q} after magneto-association of doubly occupied sites into molecules. Molecules are dark to the probe light.

Ratios of CCD measurements:

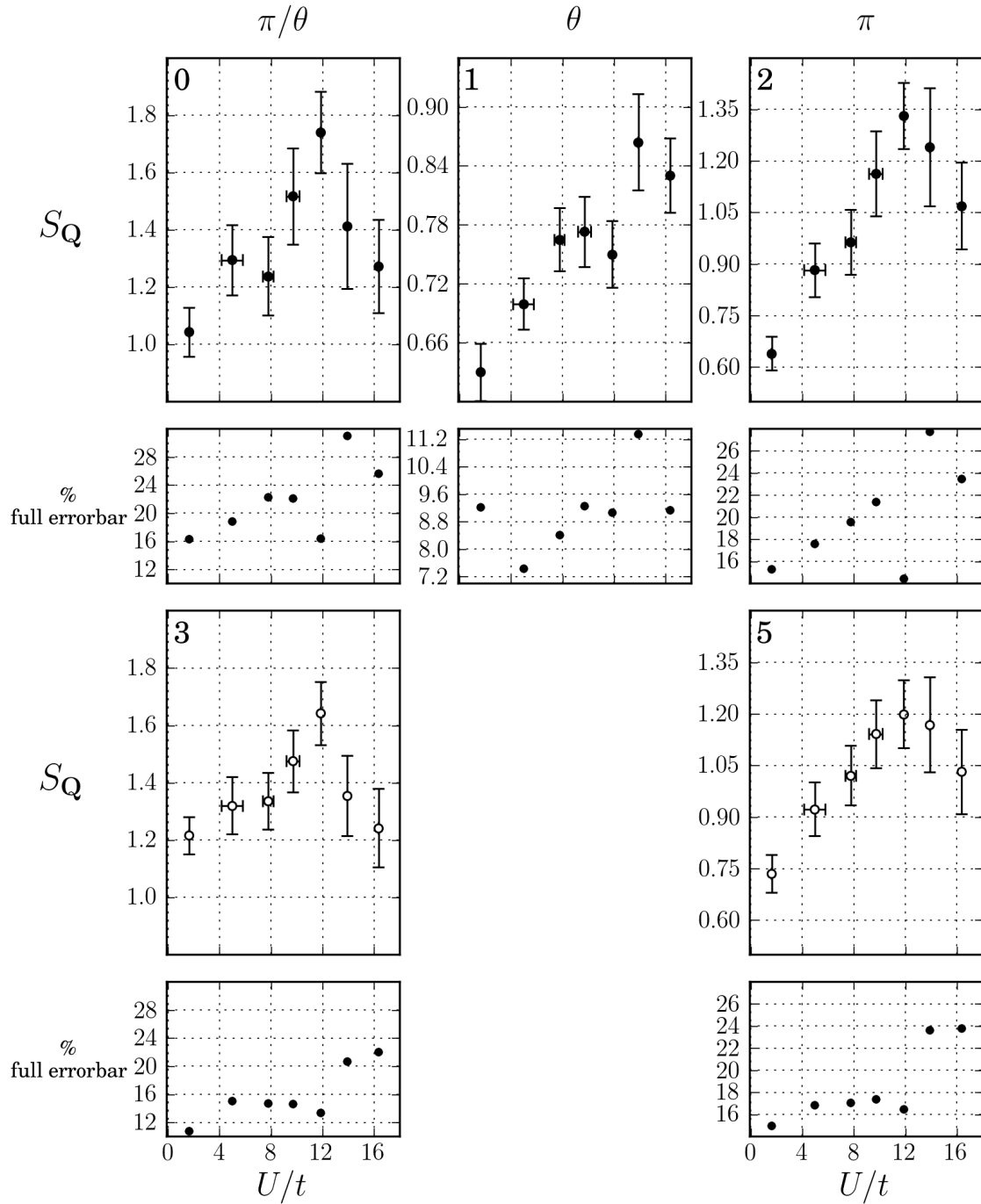
$i_{Q_{MA}}$	$\frac{I_{Q_{MA}}}{I_{Q_\infty}}$ For a given U/t the set of $I_{Q_{MA}}$ is averaged and the set of I_{Q_∞} is averaged, then the ratio is calculated.
i_S	$\frac{I_{Q_{MA\infty}}}{I_{Q_\infty}} \equiv 1 - D$, where D is the double occupancy. For a given U/t the set of $I_{Q_{MA\infty}}$ is averaged and the set of I_{Q_∞} is averaged, then the ratio is calculated.
$i_{(\pi/\theta)_{MA}}$	$\left(\frac{I_{\pi_{MA}}}{I_{\theta_{MA}}}\right) / \left(\frac{I_{\pi_\infty}}{I_{\theta_\infty}}\right)$ For a given U/t the set of $\frac{I_{\pi_{MA}}}{I_{\theta_{MA}}}$ is averaged and the set of $\frac{I_{\pi_\infty}}{I_{\theta_\infty}}$ is averaged, then the ratio is calculated.
$f_{(\pi/\theta)_{MA}}$	$\left(\frac{I_{\pi_{MA}}}{I_{\theta_{MA}}}\right) / \left(\frac{I_{\pi_\infty}}{I_{\theta_\infty}}\right)$ For a given U/t the set of $\frac{I_{\pi_{MA}}}{I_{\theta_{MA}}}$ is averaged. The set of $\frac{I_{\pi_\infty}}{I_{\theta_\infty}}$ is averaged for all data at any U/t value. This can be done since the TOF ratio depends only on the solid angle and the responsivity of the CCDs.

We use the quantities in the table above to determine the two structure factors and their ratio in the following ways:

Structure factor formulas relevant for latest data

0.	S_π/S_θ	$\frac{c_\theta}{c_\pi} \frac{i_{(\pi/\theta)_{MA}} + (c_\pi - 1)(1 - D)/i_{\theta_{MA}}}{1 + (c_\theta - 1)(1 - D)/i_{\theta_{MA}}}$	$i_{(\pi/\theta)_{MA}}$ is used.
1.	S_θ	$\frac{i_{\theta_{MA}}}{c_\theta} + \frac{c_\theta - 1}{c_\theta}(1 - D)$	For the determination of D we use $D = 1 - i_S$
2.	S_π	$\frac{i_{\pi_{MA}}}{c_\pi} + \frac{c_\pi - 1}{c_\pi}(1 - D)$	For the determination of D we use $D = 1 - i_S$
3.	S_π/S_θ	$\frac{c_\theta}{c_\pi} \frac{f_{(\pi/\theta)_{MA}} + (c_\pi - 1)(1 - D)/i_{\theta_{MA}}}{1 + (c_\theta - 1)(1 - D)/i_{\theta_{MA}}}$	$f_{(\pi/\theta)_{MA}}$ is used. This means that we use the calibration of the ratio of the two cameras, which leads to an improvement in the signal to noise ratio because common mode noise between the two cameras cancels out.
5.	S_π	$\frac{S_\pi}{S_\theta} S_\theta$	The results of 1. and 3. are combined to obtain S_π .

In the data plot shown below each panel has a number on the top left corner indicating which formula is used to obtain the data.



2.8 Comments

The first row and the third row of the plot shown above involve two different ways to get to the structure factor from our data. They are pretty close to each other within error bars but not fully consistent. We think that the most direct way to get to S_π is in the first row. The most direct way to get to the ratio S_π/S_θ is in the third row, since it uses the calibrated ratio $f_{(\pi/\theta)_{MA}}$ which only depends on the solid angle and responsivity of the cameras.

3 Sample inhomogeneity

The Quantum Monte Carlo (QMC) calculations done by the theorists in our collaboration are for systems with uniform filling, and at a fixed value of the interaction strength U/t . Our sample is far from these uniform conditions. Since it is a trapped finite sample, the filling (density) goes all the way down to zero. Typically, optical lattices are realized with laser beams that have large beam waists, so the parameters U and t have a negligible variation over the size of the sample. In our experiment we used a beam waist ($\approx 45 \mu\text{m}$) which is comparable to the size of the sample ($1/e$ radius of $\approx 20 \mu\text{m}$). For this reason we have a strong variation of U and t over the size of the sample. In our system, as you move from the center to the outside of the atom cloud the lattice gets shallower, which results in reduced U and increased t . The Hubbard interaction strength U/t thus suffers from both numerator and denominator which results in a significant variation of U/t over the cloud.

The motivation for reducing U and increasing t in length scales comparable with the sample is such that there may be entropy redistribution to the edges of the cloud. Near the edges the system has a larger entropy capacity due to the lower filling there. Additionally, since towards the edge the lattice is shallower, elastic collisions may lead to evaporation of the particles which may result in cooling of the system.

To incorporate the effects of inhomogeneity in the comparison between QMC and our measurements we will divide our sample into five bins, each with equal number of particles and then get the values of the filling n and the Hubbard parameters U and t for each of the bins. QMC calculations of the structure factor can be performed for each bin and then averaged before comparing with the experimental results.

To calculate the average value of the parameters in each bin we need knowledge of the density profile of our cloud, as well as knowledge of our optical lattice potential. The potential can be calculated from the calibrated beam waists and power of our optical lattice beams.

For the density profile we can perform in-situ phase-contrast images of the atom cloud. Alternatively, with our known atom number and the calculated potential we can use a thermodynamic model of the system to calculate the expected density distribution. The thermodynamic model we use is the high temperature series expansion up to second order in T/t , which can be calculated readily and is accurate down to about $T/t \approx 1.8$. To avoid complications with the repeatability in the realization of a certain density distribution we choose this second alternative. We feed into the model the atom number measured in the experiment. As a sanity check we can plot a particular realization of the density distribution and compare it with the calculation from the thermodynamic model. We can check if the peak density, double occupancy, and cloud size roughly agree with the model.

In Fig. 10 we show a plot of the in-situ density distribution measured using phase-contrast imaging in a $5.5 E_R$ lattice with $3.0 E_R$ of green compensation. It can be seen that the distribution is not spherically symmetric and that it has some irregularities. The $1/e$ sizes are $14 \mu\text{m}$ and $23 \mu\text{m}$. The number of atoms in the cloud is 330,000. The density at the peak is estimated from the number and the cloud sizes to be $6.45 \times 10^{12} \text{ cm}^{-3}$ which corresponds to 0.97 atoms per site. The image shown was taken at a scattering length of $380 a_0$.

If we put 330,000 atoms into the model we obtain the results shown in Fig. 11 for various values of the green compensation. The peak density and double occupancy depend sensitively on the green compensation. In order to calculate the density profiles that will be used to estimate the effect of inhomogeneity on the spin structure factor we have to pick a value for the green compensation. The value that we use in the experiment is $3 E_R$, but our observations of the peak density and the double occupancy as a function of scattering length do not match the model at $3 E_R$ compensation. Our measurement of the double occupancy in the $5.5 E_R$ lattice is shown in Fig. 12 and it resembles the curve with a compensation of $2.7 E_R$ in the model. Our measurement of the density as a function

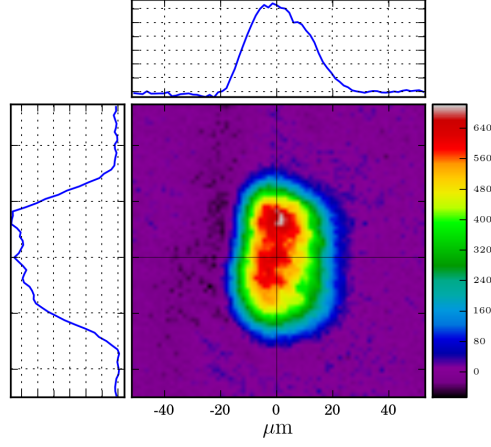


Figure 10: In-situ column density distribution in a $5.5 E_R$ lattice with $3 E_R$ of green compensation.

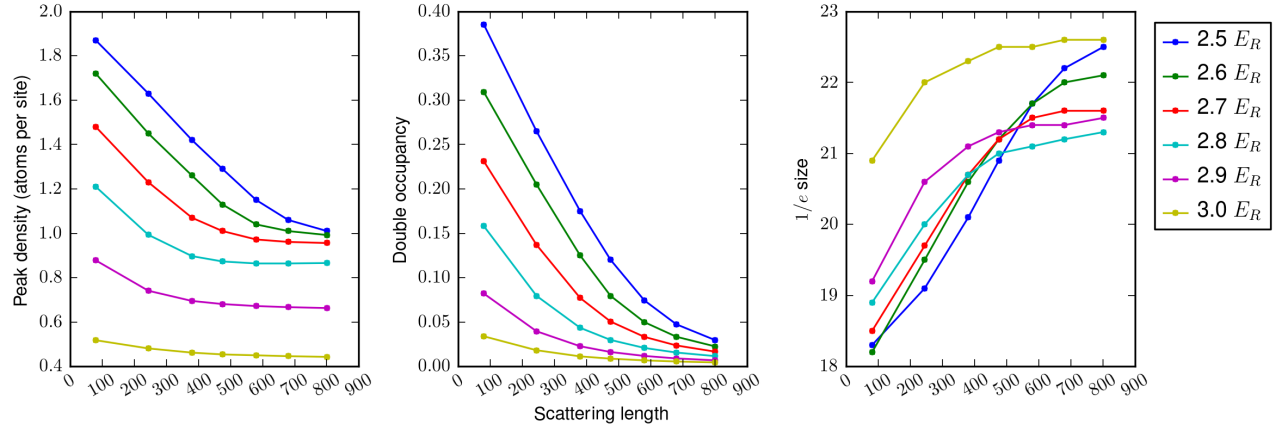


Figure 11: System parameters as a function of scattering length for various values of the green compensation. The model used is the high temperature series expansion.

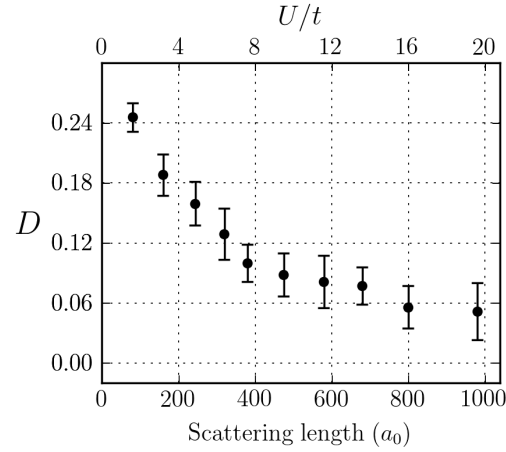


Figure 12: Double occupancy in the $5.5 E_R$ lattice.

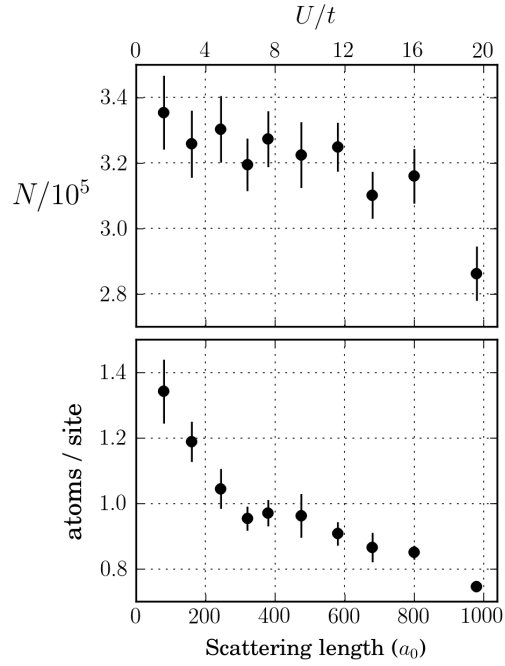


Figure 13: Peak density and atom number in the $5.5 E_R$ lattice. The plateau in the density is characteristic of the insulating state. As the scattering length is increased three-body losses become important as it is seen in both the atom number losses and decrease in the peak density.

of scattering length is shown in Fig. 13 along with the measurement of the atom number. Both the density and double occupancy measurements are consistent with a compensation of $2.7 E_R$ in the model. Discrepancies between our measurements and the model is most likely due to calibration errors and our inexact knowledge of the potential, however since the temperature used for the model is $T/t = 1.8$ it is possible that the discrepancy is also due to a lower temperature in our system than the one this model can handle. In what follows we will use $2.7 E_R$ in the model to stay consistent with our observations.

With all the parameters that go into the model in hand, we can go ahead and calculate density distributions. We then split those density distributions into bins with an equal number of atoms and calculate the filling n , and the Hubbard parameters U and t for each bin. An example of this calculation for a scattering length of $580 a_0$, which corresponds to U/t at the center equal to 11.9 is shown in Fig. 14.

In the averaging of the bins to calculate the structure factor we will assume that the entire system is isothermal at some temperature T , this corresponds to a reduced temperature T/t at the center of the sample. In a given bin, b , the reduced temperature (which will be relevant for the QMC in the bin) is given by

$$\frac{T}{t_b} = \left(\frac{T}{t} \right) \frac{t}{t_b}$$

where t is the tunneling at the center of the sample and t_b is the average tunneling in b^{th} bin.

Table 1 shows an example of the binning results for a value of $U/t = 11.86$ at the center of the sample. The table shows first the values of the parameters at the center of the sample, and then for each bin the columns show respectively n_b , t/t_b , and U_b/t_b . These three values are what is needed to perform the QMC calculation in each bin.

Below, in Table 2, we produce seven tables like Table 1 for the seven different values of U/t at the center that correspond to our structure factor data in the $5.5 E_R$ lattice. We add a column labeled u , which corresponds to the ratio of U_b/t_b to U/t at the center.

$$V_L = 5.50, V_G = 2.70, a_s = 580, U/t = 11.8, T/t = 1.8, N = 3.28 \times 10^5$$

Sample is divided in 5 bins, all containing the same number of atoms (see panel 2).

Average Fermi-Hubbard parameters n , U , t , and U/t are calculated in each bin (see panels 1, 3, 4, 5)

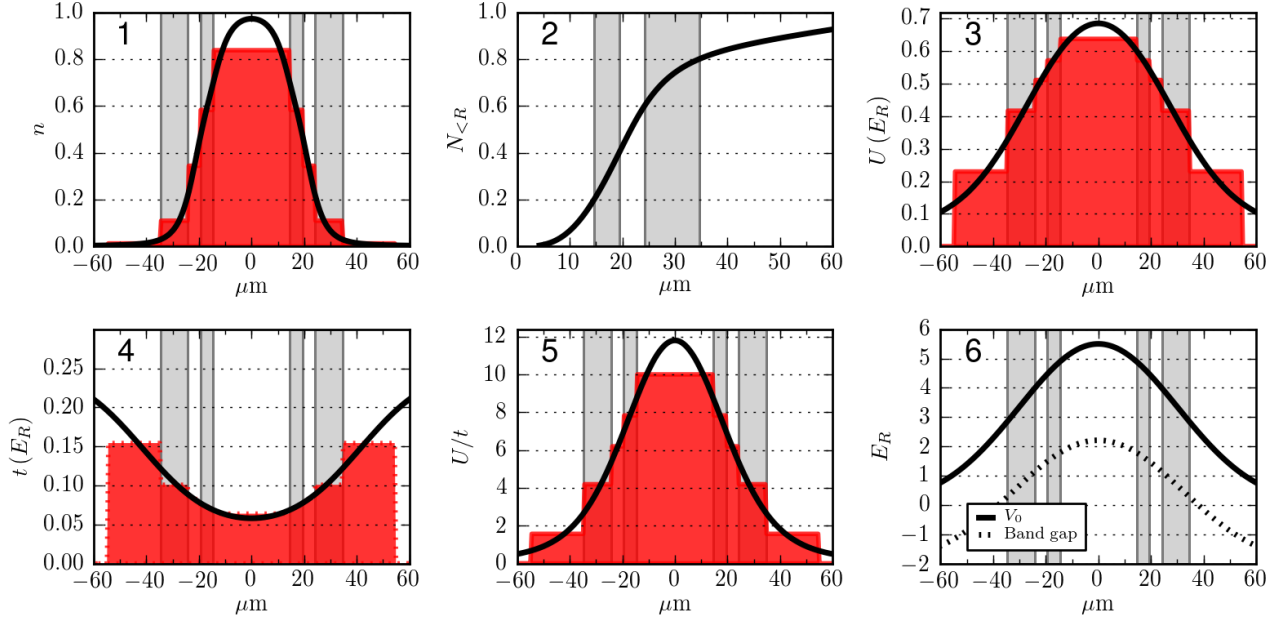


Figure 14: Binned filling and Hubbard parameters are shown in panels 1, 3, 4, and 5. The average value in each bin is shown as the shaded red area. The cumulative number up to a certain radius is shown in panel 2, this illustrates how all the bins have the same number of atoms. The lattice depth and band gap as a function of radius are shown in panel 6.

At center:

$$t = 0.058 \text{ Er}$$

$$U = 0.687 \text{ Er}$$

$$U/t = 11.860 \text{ Er}$$

At bins:

bin#	nb	t/tb	U/tb
<hr/>			
000	0.84	0.91	9.97
001	0.58	0.79	7.82
002	0.34	0.70	6.19
003	0.11	0.57	4.13
004	0.01	0.38	1.49

Table 1: Binning for $U/t = 11.86$

At center:				
t = 0.058 Er				
U = 0.095 Er				
U/t = 1.636 Er				
At bins:				
bin#	nb	t/tb	Ub/tb	u
000	1.18	0.93	1.42	0.87
001	0.79	0.83	1.17	0.71
002	0.45	0.74	0.95	0.58
003	0.14	0.62	0.67	0.41
004	0.02	0.41	0.27	0.17
At center:				
t = 0.058 Er				
U = 0.288 Er				
U/t = 4.976 Er				
At bins:				
bin#	nb	t/tb	Ub/tb	u
000	0.99	0.91	4.25	0.86
001	0.66	0.81	3.41	0.69
002	0.39	0.72	2.75	0.55
003	0.12	0.60	1.90	0.39
004	0.02	0.40	0.73	0.16
At center:				
t = 0.058 Er				
U = 0.450 Er				
U/t = 7.771 Er				
At bins:				
bin#	nb	t/tb	Ub/tb	u
000	0.89	0.91	6.54	0.84
001	0.61	0.80	5.19	0.67
002	0.37	0.71	4.17	0.54
003	0.12	0.59	2.83	0.37
004	0.01	0.39	1.05	0.14
At center:				
t = 0.058 Er				
U = 0.563 Er				
U/t = 9.713 Er				
At bins:				
bin#	nb	t/tb	Ub/tb	u
000	0.85	0.91	8.17	0.84
001	0.60	0.80	6.48	0.67
002	0.36	0.71	5.14	0.53
003	0.11	0.58	3.42	0.36
004	0.01	0.38	1.27	0.14
At center:				
t = 0.058 Er				
U = 0.687 Er				
U/t = 11.860 Er				
At bins:				
bin#	nb	t/tb	Ub/tb	u
000	0.84	0.91	9.97	0.84
001	0.58	0.79	7.82	0.66
002	0.34	0.70	6.19	0.52
003	0.11	0.57	4.13	0.35
004	0.01	0.38	1.49	0.13
At center:				
t = 0.058 Er				
U = 0.806 Er				
U/t = 13.905 Er				
At bins:				
bin#	nb	t/tb	Ub/tb	u
000	0.83	0.91	11.69	0.84
001	0.58	0.79	9.17	0.66
002	0.35	0.70	7.25	0.52
003	0.11	0.57	4.84	0.35
004	0.01	0.38	1.75	0.13
At center:				
t = 0.058 Er				
U = 0.948 Er				
U/t = 16.359 Er				
At bins:				
bin#	nb	t/tb	Ub/tb	u
000	0.83	0.91	13.78	0.84
001	0.57	0.79	10.80	0.66
002	0.33	0.70	8.43	0.52
003	0.10	0.57	5.51	0.34
004	0.01	0.37	1.98	0.13

Table 2: Binning for various values of U/t

bin#	nb	t/tb	u
000	0.92	0.91	0.85
001	0.63	0.80	0.67
002	0.37	0.71	0.54
003	0.12	0.59	0.37
004	0.01	0.39	0.14

Table 3: Binning for general case. To estimate the trap averaged structure factor at a temperature $T/t \equiv x$ and with an interaction given by $U/t \equiv y$, a QMC calculation will be performed for each bin using filling nb , temperature $x(t/t_b)$ and interaction strength yu .

We point out that the n , t/t_b and u columns do not differ much across the different values of U/t at the center. To simplify the matter, and since this treatment is only a crude estimation we create a single table, Table 3, which averages the binnings for the seven values of U/t at the center. In this way we obtain a binning with which we can represent the inhomogeneity of our sample in a general case.

3.1 Raw data for S_π/S_θ and S_π

Below we show the raw data for the best estimate of S_π/S_θ which uses the simultaneous measurement of both cameras with a calibrated normalization. This is panel 3 on the figure with the data.

U/t	Spi/St _θ	error
1.6	1.21	0.065
5.0	1.32	0.099
7.8	1.34	0.098
9.7	1.48	0.108
11.9	1.64	0.110
13.9	1.35	0.140
16.4	1.24	0.136

Below we show S_π determined from S_π/S_θ and S_θ , this is panel 5 on the figure with the data .

U/t	Spi	error
1.6	0.735	0.055
5.0	0.923	0.078
7.8	1.021	0.087
9.7	1.141	0.099
11.9	1.199	0.099
13.9	1.168	0.138
16.4	1.031	0.123

Below we show S_π determined using only the camera at π , this is panel 2 on the figure with the data.

U/t	Spi	error
1.6	0.639	0.049
5.0	0.882	0.078
7.8	0.963	0.094
9.7	1.162	0.124
11.9	1.331	0.096
13.9	1.240	0.172
16.4	1.069	0.125

References

- [1] R. Loudon, *The Quantum Theory of Light, Oxford Science Publications* (OUP Oxford, 2000).
- [2] C. Cohen-Tannoudji, J. Dupont-Roc, and G. Grynberg, *Atom-Photon Interactions: Basic Processes and Applications, A Wiley-Interscience publication* (Wiley, 1998).